Energy & Environmental Science

REVIEW

View Article Online
View Journal | View Issue

Cite this: *Energy Environ. Sci.*, 2017, **10**, 710

The rapid evolution of highly efficient perovskite solar cells

Juan-Pablo Correa-Baena,†*[a] Antonio Abate,*[b] Michael Saliba,*[c] Wolfgang Tress,[c] T. Jesper Jacobsson,[d] Michael Grätzel[c] and Anders Hagfeldt[a]

Received 21st November 2016,
Accepted 30th January 2017

DOI: 10.1039/c6ee03397k

rsc.li/ees

Perovskite solar cells (PSCs) have attracted much attention because of their rapid rise to 22% efficiencies. Here, we review the rapid evolution of PSCs as they enter a new phase that could revolutionize the photovoltaic industry. In particular, we describe the properties that make perovskites so remarkable, and the current understanding of the PSC device physics, including the operation of state-of-the-art solar cells with efficiencies above 20%. The extraordinary progress of long-term stability is discussed and we provide an outlook on what the future of PSCs might soon bring the photovoltaic community. Some challenges remain in terms of reducing non-radiative recombination and increasing conductivity of the different device layers, and these will be discussed in depth in this review.

Broader context

Perovskite-based solar cells have emerged as a promising technology for highly efficient and low-cost photovoltaics. Using low-temperature solution processing, the high efficiencies so far reported go beyond 20% and start approaching their practical limitations. This unprecedented rise in efficiency, with the added advantage of low-cost processing, has made perovskite solar cells an exciting field of study. In this review, we summarize some of the major developments in the perovskite field related to thin film material processing, solar cell physics and long-term stability, which are key to commercialization of this exciting technology.

1. Introduction

One of the hottest topics in materials science in the past few years has been hybrid organic–inorganic perovskites, which have risen to stardom due to their remarkable properties in opto-electronic applications. In particular, they have revolutionized the field of photovoltaics, with spectacular achievements in power conversion efficiencies that rival silicon and other established thin-film technologies (*i.e.* CdTe and CIGS). With more than 2000 publications on the subject in just a few years, perovskite solar cells (PSCs) have evolved and matured quickly. First, the efficiencies are as high as is necessary for commercialization. Then, the fundamental properties of the material have been properly established. The main debate of the field on hysteresis and ferroelectricity has been debunked. Coupled with remarkable stability and rapid progress in upscaling (*i.e.* modules and processing), this review will provide an overview of the latest developments in this rapidly evolving field.

PSCs composed of organic-metal-halide materials have made impressive progress in just a few years with maximum power conversion efficiencies (PCEs) evolving from 3.8%[1] in 2009 to a certified 22.1%[2] in 2016. In the past year, huge progress has been shown for different device configurations, including the classic mesoporous-infiltrated *n–i–p* junction and mesoporous-free "planar" configurations. The latter are low temperature-processed SnO_2-based configurations, which can now yield efficiencies close to the high temperature-processed mesoporous analogues.[3,4] Monolithic tandem c-Si/perovskite solar cells have shown tremendous progress, achieving high efficiencies above 25%[5] with a potential of above 30%[6] with further optimization. Additionally, industry friendly deposition techniques have been developed recently,[7] bridging the gap between academic research and its industrial partners.

The past two years have also proven to be of paramount importance in understanding the transient phenomena that have dominated the discussion of measuring the real power conversion efficiency.[8–13] Ionic movement modifying the electric

[a] *Laboratory of Photomolecular Science, Institute of Chemical Sciences and Engineering, École Polytechnique Fédérale de Lausanne, CH-1015-Lausanne, Switzerland. E-mail: juan.correa@epfl.ch*
[b] *Adolphe Merkle Institute, Chemin des Verdiers 4, CH-1700 Fribourg, Switzerland. E-mail: antonio.abate@unifr.ch*
[c] *Laboratory for Photonics and Interfaces, Institute of Chemical Sciences and Engineering, École Polytechnique Fédérale de Lausanne, CH-1015-Lausanne, Switzerland. E-mail: michael.saliba@epfl.ch*
[d] *Christian Doppler Laboratory for Sustainable Syngas Chemistry, Department of Chemistry, University of Cambridge, Lensfield Road, Cambridge, UK*
† Current address: Massachusetts Institute of Technology, Cambridge, MA, USA.

field in the device is now widely accepted as the main mechanism that causes hysteresis in the current–voltage curves under working conditions. To properly address the issue of hysteresis, slow scan rates have been suggested to yield steady-state efficiencies. However, maximum power point tracking has been established as the most accurate way to measure the real steady state efficiency of perovskite solar cells.

While progress has been related mostly to the short-term performance of devices, very little attention has been paid so far to their long-term implications. In the past year, however, there has been a push towards further understanding of the mechanisms that drive the stability of PSCs, with rapid progress towards long-term stable devices.

Here, we review the rapid evolution of PSCs as these enter a new phase that could revolutionize the photovoltaic industry. In particular, we describe the properties that make perovskites so remarkable, and the current understanding of the PSC device physics, including the operation of state-of-the-art solar cells with efficiencies above 20%. Finally, we discuss the extraordinary progress of long-term stability, and the evolution towards modules, and provide an outlook on what the future of PSCs might soon bring the photovoltaic (PV) community.

2. Perovskite properties and processing

Structural features

The perovskite structure, with composition ABX_3, was first described by Goldsmith in the 1920s in work relating to

Juan-Pablo Correa-Baena

Juan-Pablo Correa-Baena is a postdoctoral researcher in the group of Prof. Tonio Buonassisi at MIT. He spent 2 years as a postdoctoral researcher in the group of Prof. Anders Hagfeldt at the EPFL. He pursued his PhD at UCONN, USA, on a National Science Foundation scholarship. His thesis work focused on the study of porous metal oxides, applied in dye-sensitized solar cells. At EPFL he worked on perovskite solar cell research focusing on understanding the interfacial dynamics between perovskites and the electron and hole selective layers and developing new strategies to improve efficiency in planar perovskite solar cells.

Antonio Abate

Antonio Abate is a research group leader at the Helmholtz-Zentrum Berlin. He is an expert in hybrid organic–inorganic materials for optoelectronics. His group is currently researching active materials and interfaces to make stable perovskite solar cells. Before moving to the Helmholtz-Zentrum Berlin, Antonio was leading the solar cell research at the Adolphe Merkle Institute and he was a Marie Skłodowska-Curie Fellow at École Polytechnique Fédérale in Switzerland. After getting his PhD at Politecnico di Milano in 2011, he worked for 4 years as a postdoctoral researcher at the University of Oxford and the University of Cambridge.

Michael Saliba

Dr Michael Saliba is a Marie Curie Fellow at EPFL. He completed his PhD at Oxford University in 2014 working on crystallization behaviour and plasmonic nanostructures in perovskites. He completed his MSc in physics at the Max Planck Institute for Solid State Research on simulation methods for plasmonic oligomers. He holds a BSc in mathematics and physics from Stuttgart University. His research focuses on a deeper understanding and improvement of the optoelectronic properties of emerging photovoltaic technologies with an emphasis on perovskites for a sustainable energy future. In 2016, he was awarded the Young Scientist Award of the German University Association.

Wolfgang Tress

Wolfgang Tress is currently working as a scientist at LPI, EPFL in Switzerland, with general interests in developing and studying novel photovoltaic concepts and technologies. His research focuses on the device physics of perovskite solar cells, most recently, investigating recombination and hysteresis phenomena in this emerging material system. Previously, he was analyzing and modeling performance limiting processes in organic solar cells.

tolerance factors[14] and lends its name from $CaTiO_3$. The ideal structure has cubic symmetry and is composed of a backbone of corner sharing BC_6-octahedra with cuboctahedral voids occupied by the A-cations (Fig. 1a–c). If the A-ion is small, or the B-ion is large, the tolerance factor (t) decreases below 1 and orthorhombic, rhombohedral, or tetragonal structures are favoured rather than the ideal cubic structure. For large A-ions, layered 2D structures[15,16] and 1D chain materials[17] are known, and a large number of superstructures, compositions, and stoichiometries have been described,[18] *e.g.* Ruddlesden–Popper, Aurivillius, and Dion–Jacobson phases.[19] The layered 2D-structures have attracted attention for various applications, but it is the 3D-perovskites that have recently gained the attention of the solar cell community. More recently, 2D and mixtures of 2D and 3D have attracted attention due to their increased robustness to moisture compared to their pure 3D counterparts.[20,21]

There is a large class of related perovskite compounds with promising PV-characteristics. Out of those, methyl ammonium lead iodide, $CH_3NH_3PbI_3$ (or $MAPbI_3$), has been most extensively investigated and can therefore be seen as a standard perovskite and a model compound. In terms of high efficiency devices, attention has now shifted away from $MAPbI_3$ towards mixed ion perovskites ($FA_xMA_{1-x}PbBr_yI_{3-y}$).

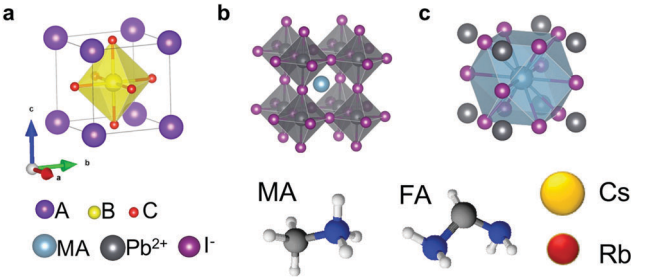

Fig. 1 Structural features of metal halide perovskite materials. (a) Unit cell of a general cubic perovskite. (b) $MAPbI_3$ illustrating the octahedral coordination around the lead ions. (c) $MAPbI_3$ illustrating the cuboctahedra coordination around the organic ion.

Given the ionic radii (Pb^{2+} = 0.132 nm, I^- = 0.206, and $CH_3NH_3^+$ = 0.18 nm[22]), the tolerance factor suggests that $MAPbI_3$ should form a tetragonal structure, with PbI_6-octahedra as the backbone with MA-ions occupying the cuboctahedral voids between them. This is consistent with single crystal data finding $MAPbI_3$ in the tetragonal space group *I4cm* at room temperature.[23] At −113 °C, a phase transition to an orthorhombic phase (space group *Pnma*) has been observed.[24–27] This phase does not appear to work well for PV applications[28] but as this temperature is not experienced in terrestrial environments, it is of no practical concern. As the temperature rises and the thermal energy increases, perovskites commonly go towards a more cubic symmetry. For $MAPbI_3$, a transition from tetragonal to cubic (or pseudocubic[29]) symmetry occurs at around 54 °C.[27,29–31] This is well within the operational window of solar cells and can thus potentially affect the performance of a photovoltaic device. However, the phase transition is slow[30,32] and reversible,[30] and seems not to be problematic for PV applications.[28]

T. Jesper Jacobsson

Dr T. J. Jacobsson was awarded a PhD in inorganic chemistry from Uppsala University in 2014 for work on the size dependent properties of ZnO quantum dots and CIGS-based devices for solar hydrogen production. In 2015, he moved to EPFL and the Laboratory of Photomolecular Science where he focused on the physical properties and synthesis of high efficiency lead halide perovskite solar cells. He is currently undertaking a second postdoc at the University of Cambridge, focusing on perovskite solar cells and inorganic catalysts for hydrogen production.

Michael Grätzel

Michael Grätzel studied Chemistry and received a doctoral degree in natural science from the Technical University Berlin. Professor of Physical Chemistry at the Ecole Polytechnique Fédérale de Lausanne (EPFL) since 1977, he directs there the Laboratory of Photonics and Interfaces, conducting research on energy and electron transfer reactions in mesoscopic systems and their use to generate electricity and fuels from sunlight. His recent awards include the Centenary Prize of the Royal Society of Chemistry, the Benoist Prize, the Albert Einstein World Award of Science, the Paul Karrer Gold Medal, as well as the Millennium Technology Grand Prize, and the Balzan Prize.

Anders Hagfeldt

Anders is a Professor in Physical Chemistry at EPFL, Switzerland. He obtained his PhD at Uppsala University in 1993 and was a post-doc with Prof. Michael Grätzel (1993–1994) at EPFL. His research focuses on the fields of dye-sensitized and perovskite solar cells, and solar fuels. He has published more than 400 articles with over 36 000 citations (h-index 95). He is a member of the European Academy of Sciences, Royal Swedish Academy of Sciences, Royal Society of Sciences in Uppsala, and the Royal Swedish Academy of Engineering Sciences. He is a visiting professor at Uppsala University and Nanyang Technological University, Singapore.

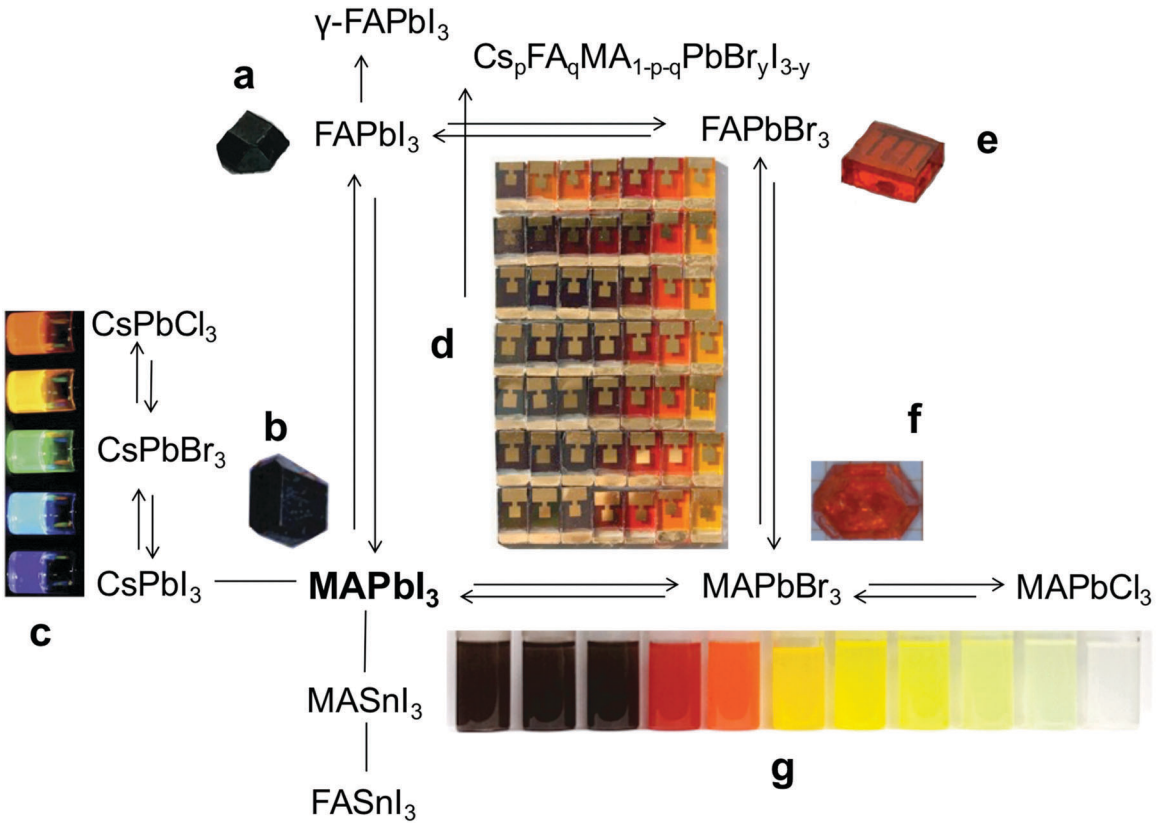

Fig. 2 The versatility of hybrid perovskite materials and their absorption tunability. Schematics of some investigated perovskites closely related to $MAPbI_3$. The insets show (a) single crystal of $FAPbI_3$, reprinted with permission,[33] (b) single crystal of $MAPbI_3$, reprinted with permission,[34] (c) colloidal solutions of $CsPbX_3$ (X = Cl, Br, I) perovskites, reprinted with permission,[35] (d) solar cells of 49 different compositions in the MA/FA-Pb-Br/I compositional space, reprinted with permission,[36] (e) single crystal of $FAPbBr_3$, reprinted with permission,[33] (f) single crystal of $MAPbBr_3$, reprinted with permission[34] and (g) colloidal nanocrystals of $MAPbX_3$ (X = Cl, Br, I) perovskites, reprinted with permission.[37]

Halide substitution

One of the biggest advantages of the metal halide perovskites is the ability to tune their optoelectronic properties by ion substitution. The iodine in $MAPbI_3$ can be replaced with both chlorine and bromine,[38] and large single crystals have been grown from all three halide perovskites: $MAPbCl_3$, $MAPbBr_3$, and $MAPbI_3$[39] (Fig. 2). While the ionic size of the halide decreases, the band gap increases and for single crystals it is found to be 2.97, 2.24, and 1.53 eV for the Cl, Br, and I perovskite, respectively.[39] The values measured for polycrystalline films are generally somewhat higher,[40,41] *i.e.* 3.1 and 2.3 eV for the Cl and Br perovskite[38] and 1.6 for the I-perovskite.[36] From a photovoltaic perspective, $MAPbI_3$ is thus suitable for single band gap absorbers and $MAPbBr_3$ could be interesting for tandem applications whereas $MAPbCl_3$ is relevant to light emitting devices. Both the chloride and the bromide perovskite are found in a cubic structure (*Pm3m*) at room temperature[38] with transitions to a tetragonal structure at lower temperatures, *i.e.* −119 °C for $MAPbCl_3$[42] and −62 °C for $MAPbBr_3$.[24]

Monovalent organic cation substitution

Also the cation can be replaced and MA has successfully been exchanged by the slightly larger formamidinium ion $(CH(NH_2)_2)^+$ or FA).[43,44] The cation exchange only has a small impact on the optical band gap. This is in line with DFT computations which demonstrate that MA/FA does not contribute to electronic states close to the band edges.[45,46] The larger FA ion does, however, expand the lattice[36] and change the tilt of the PbI_6-octahedra[47] which results in a slight decrease of the band gap from ~1.59 eV for $MAPbI_3$[36] to ~1.45–1.52 eV for $FAPbI_3$.[36,43] From the perspective of light absorption, this is a more suitable band gap for a single junction PV device. At room temperature, $FAPbI_3$ is found in a cubic[48] or a tetragonal structure (*P3m1*) very close to cubic.[49] The experimentally observed phase pure structure is typically formed at higher temperature annealing than for the MA-based analogues.[50] One major issue, however, is that the large size of FA results in a higher energy barrier for intercalation between the PbI_2 layers during perovskite formation. This can be somewhat offset by a higher annealing temperature.[36,43] Additionally, the cubic (or pseudocubic) α-phase at room temperature easily transforms into a yellow polymorph with hexagonal symmetry (*P63mc*) unsuitable for PV-applications.[29,50,51]

Organic/inorganic ion mixing

Simultaneous exchange of both MA to FA and I to Br has been done as well. $FAPbBr_3$ has a cubic or pseudocubic structure[52] and a band gap of ~2.3 eV[36] which could be interesting for

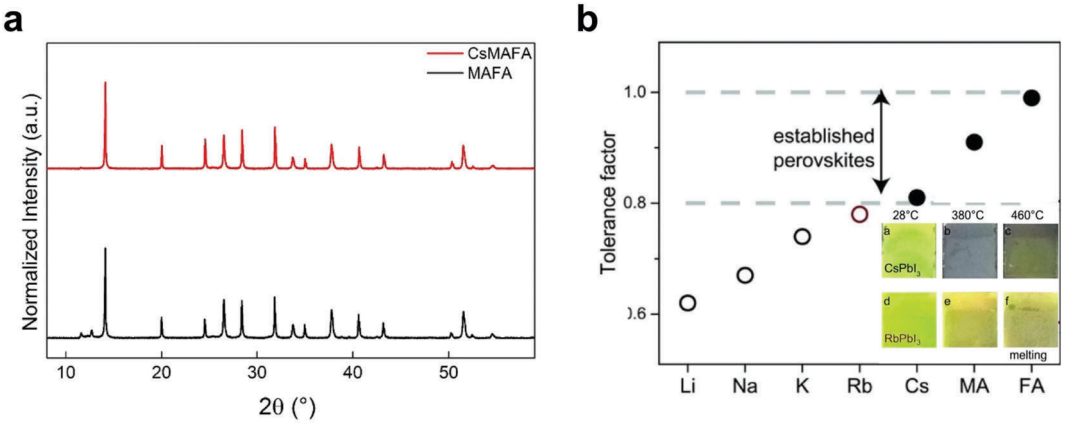

Fig. 3 Organic–inorganic cation incorporation into the perovskite structure (a) XRD of a mixed MA/FA perovskite and that with the incorporation of Cs, reprinted with permission.[62] (b) Tolerance factor of $APbI_3$ perovskite with the oxidation-stable A = Li, Na, K, Rb, Cs; and MA, and FA, reprinted with permission.[63] Empirically, perovskites with a tolerance factor between 0.8 and 1.0 (dashed lines) show a photoactive black phase (solid circles with Cs, MA, and FA depicted below) as opposed to non-photoactive phases (open circles). Rb (red open circle) is very close to this limit making it a candidate for integration into the perovskite lattice. The inset shows $CsPbI_3$ (first row) and $RbPbI_3$ (second row) at 28 °C, 380 °C, and 460 °C. Irreversible melting for both compounds occurs at 460 °C. $RbPbI_3$ never shows a black phase.

tandem applications. Using perovskites with mixed cations and halides is an important theme because the pure perovskite compounds suitable for PV applications come with numerous disadvantages. For example, $MAPbI_3$ has never reached stabilized efficiencies beyond 20%.[53] On the other hand, $FAPbI_3$ and $CsPbI_3$ are not stable in the cubic (or pseudocubic) α-phase at room temperature. The entire compositional space of MA/FA/Br/I-Pb perovskites has been mapped experimentally.[36] FA appears to give advantages over MA, but some MA stabilises the perovskite structure and prevents it from transforming into the yellow polymorph known for the FA perovskites.[32,42,54] Introducing Br allows for tuning of the band gap, which is favourable for tandem applications, and some Br appears to be favourable for the device performance. The precise composition can have a large impact on the final device performance and the best cells, which have up to 21% efficiency, are found for compositions around $FA_{2/3}MA_{1/3}Pb(Br_{1/3}I_{2/3})_3$.[36,55,56] Too much Br (about 50%) leads to stability problems and a partial phase segregation may occur, which leads to small inclusions of a more iodine rich phase acting as efficient recombination centres.[36] For the $MAPbBr_xI_{3-x}$-series, simulations indicate that a large window in the compositional mixture may be thermodynamically unstable at room temperature with respect to phase separation.[57]

Therefore, it has become an important design principle to mix cations and halides to achieve perovskite compounds combining the advantages of the constituents while avoiding their drawbacks. The recent success of the double-cation MA/FA mixtures demonstrates that a small amount of MA already induces a preferable crystallization of FA perovskite into its photoactive black phase resulting in a more thermally and structurally stable composition than pure MA or FA compounds.[56,58]

The same holds true for Cs/FA[59,60] mixtures which additionally suppress halide segregation enabling intermediate band gaps for tandem applications.[61] Finally, following this approach further Cs/MA/FA triple cation perovskites were synthesized to improve crystal quality.[62] This is shown in Fig. 3, where an XRD pattern of a double-cation MAFA perovskite is depicted. It shows that the detrimental, photoinactive "yellow phase" impurities are present. Adding Cs results in a substantially suppressed "yellow phase". The triple cation direction was guided by the choice of cations (Cs, MA, and FA) which were well-known to have a photoactive black phase perovskite. Recently, a less obvious cation was successfully used: the seemingly too small Rb that does not have a photoactive black phase when used as a single-cation $RbPbI_3$ compound.[63] Empirically, the perovskites with a black phase that are of interest for PV application fulfil $0.8 < t < 1.0$ as illustrated in Fig. 3 where the tolerance factor of an $APbI_3$ structure is shown with A being Li, Na, K, Rb, Cs, MA, and FA. Only the single-cation Cs, MA, and FA are "established perovskites" with a black phase and reports of high efficiency PSCs. The alkali metals are particularly attractive because of their inherent oxidation-stability. This is illustrated further in Fig. 3 (inset) where only $CsPbI_3$ but not $RbPbI_3$ has a black phase showing that Cs and Rb are indeed the demarcation line between photoactive and photoinactive perovskites.

Lead-free perovskites

Replacing lead would be favourable from both a toxicological and a legalisation perspective, and attempts have been made with a few different elements.[46,64–67] Most effort has been directed towards tin perovskites,[68,69] and efficiencies up to 6% have been demonstrated for $MASnI_3$.[68] The toxicological profile of a water soluble tin perovskite is, however, not entirely unproblematic either,[70] and due to the lack of the inert pair effect, Sn^{2+} is easily oxidised to Sn^{4+} which is detrimental for the stability and the structural integrity of the perovskite.[68,69] Alloying of Sn/Pb perovskites has become an important route towards more optimal bandgaps, with recent breakthroughs reported to yield high efficiencies up to 15%, despite their low tolerance to environmental oxygen.[71] Tandem structures using perovskites of narrow bandgaps (Sn/Pb alloys) coupled with wide bandgaps have also been investigated as potential systems.[72,73]

Bi-based compounds have also attracted some attention recently with various works showing their potential.[64,74,75] A more broad approach for identifying defect-tolerant materials similar to Pb-based perovskites has also been described by Brandt *et al.*[76]

Perovskite processing

The dominating approach to $MAPbI_3$ synthesis is wet chemical deposition which could be divided into either one or two-step protocols. In the latter, PbI_2 is deposited in a first step and then exposed to the organic ions, either in solution[77] or in vapour,[78] whereupon organic ions are intercalated between the layers of edge sharing PbI_6 octahedra and form the perovskite.[68,79] Under thermal stress, the reversed mechanism occurs and MA dissipates as vapour, leaving PbI_2 behind.[79,80] The MA ion is smaller than the FA ion which facilitates the intercalation and for pure $FAPbI_3$, a higher temperature is needed for the intercalation to occur.[18,22] In one-step protocols, the precursor salts are dissolved in polar solvent mixtures typically in a single container. A subclass of one step methods, known as the anti-solvent method,[81] was introduced in 2014.[82,83] A perovskite precursor solution is then spin-coated, but during the spinning program an anti-solvent, *e.g.* chlorobenzene or toluene, is poured on top of the spinning film. This facilitates crystallisation and generates a good film morphology. The best cells are at the moment produced using anti-solvent protocols. A drawback is the level of artisanship involved and it may be hard to scale up.[84] A possible way around insufficient homogeneity after deposition is to recrystallize the deposited films in DMF vapour as a post deposition treatment which has been done with some success.[85,86]

The crystallisation dynamics in the anti-solvent method appears to be heavily dependent upon the precise conditions under which it is performed. Under certain conditions, it is probably essentially the same as in the 2-step protocols where PbI_2, which has a lower solubility, precipitates and then is intercalated by the organic ions. A recrystallization route is also possible and in iodine rich environments, PbI_3^- and PbI_4^{2-} complexes have been identified as intermediates.[87] The solvent plays a role as well and the best devices are generally obtained with mixtures of DMF and DMSO, as compared to pure DMF.[88] This leads to bound intermediates with DMSO and PbI_2[89] or even polymeric plumbate(II) fibers.[90] This interaction is described as a Lewis-base adduct[82,91,92] and forms an intermediate phase upon solvent removal before the perovskite forms under thermal annealing,[84] and this influences both the film morphology and the crystal grain size. Part of this intermediate phase may also be left in the perovskite film after thermal annealing without immediate negative effects on the device performance.[93]

The perovskite crystal quality is very important for high photovoltaic performance; however, there are additional factors that are important from a device perspective. Grain boundaries and the defect chemistry play an important role, for instance. The remnant PbI_2 in perovskite films has been found to yield better performing devices.[53,55,94–96] A number of hypotheses have been discussed,[97] most of them based on interface passivation. The benefit was, however, not found to be unequivocal as also a deficiency of PbI_2 could have beneficial effects.[97,98] It turns out that a surplus of MA in the synthesis could lead to a more complete conversion of PbI_2 into the perovskite. This leads to higher crystal core qualities, longer lifetimes, and open circuit voltages as high as 1.2 V.[97] On the other hand, this decreased the favourable grain boundary characteristics that were found in the PbI_2 rich perovskites and decreased the overall cell performance. An increased focus on how to control the grain boundary characteristics and the precise stoichiometry for getting more stable devices with higher performance is likely going to be a focus area in the years to come.

3. Device architectures and the rapid efficiency evolution

PSCs have been traditionally designed with the use of a mesoporous scaffold and a stack architecture as seen in Fig. 4a and b. These are composed of fluorine-doped tin oxide (FTO), an electron transport/selective layer (ETL) often in the form of a mesoporous scaffold of different thicknesses, the perovskite material, either infiltrated in the mesoporous scaffold or as a "capping" layer atop the ETL, and a hole selective/transport layer (HSL) with a metal contact. Scanning electron mircrographs (SEMs) of state-of-the-art PSCs (efficiency above 20%) are shown for the TiO_2 mesoporous (Fig. 4b) and SnO_2 planar (Fig. 4c) configurations. An additional planar configuration has been developed where the stack described above is inverted (TCO/HTL/Perovskite/ESL/Metal),[99–105] however, this configuration will not be the focus in this review as all record high efficiencies, and most of the PSC studies have been performed on the "traditional" FTO/ETL/Perovskite/HSL/Metal configurations.

Mesoporous infiltrated and perovskite-capped devices

PSCs were pioneered in a dye-sensitized solar cell (DSC) configuration in 2009 where Kojima and coworkers[1] used a thick mesoporous TiO_2 (8–12 μm), and infiltration of the perovskite materials based on I or Br in combination with a liquid electrolyte. Subsequent work on mesoporous scaffold configurations, mostly composed of TiO_2, yielded record efficiencies up to 22.1%.[114] The highest efficiency reported each year is plotted in Fig. 4d, where the impressive increase in efficiency is shown from 3.8 to 22.1% in only 7 years. The second work on PSCs was published in 2011 (no PSC work was published in 2010) and also used a DSC configuration with a liquid electrolyte yielding 6.5% efficiency.[107] A breakthrough in PSCs arrived with the introduction of a solid state HTL (Spiro-OMeTAD) by Kim *et al.*[115] and Lee *et al.*,[108] which, unlike the liquid analogues, did not dissolve the perovskite layer, and thus opened up the field for exploration. Since then, a series of efficiency records have been progressively published. During the first few years (Fig. 4d, shaded in grey), as will be discussed in the next section, *J–V* hysteresis (a phenomenon of different efficiencies depending on the scan direction, forward or backward) was not accounted for and non-stabilized efficiencies were measured. In the past 2 years, efforts have been made to

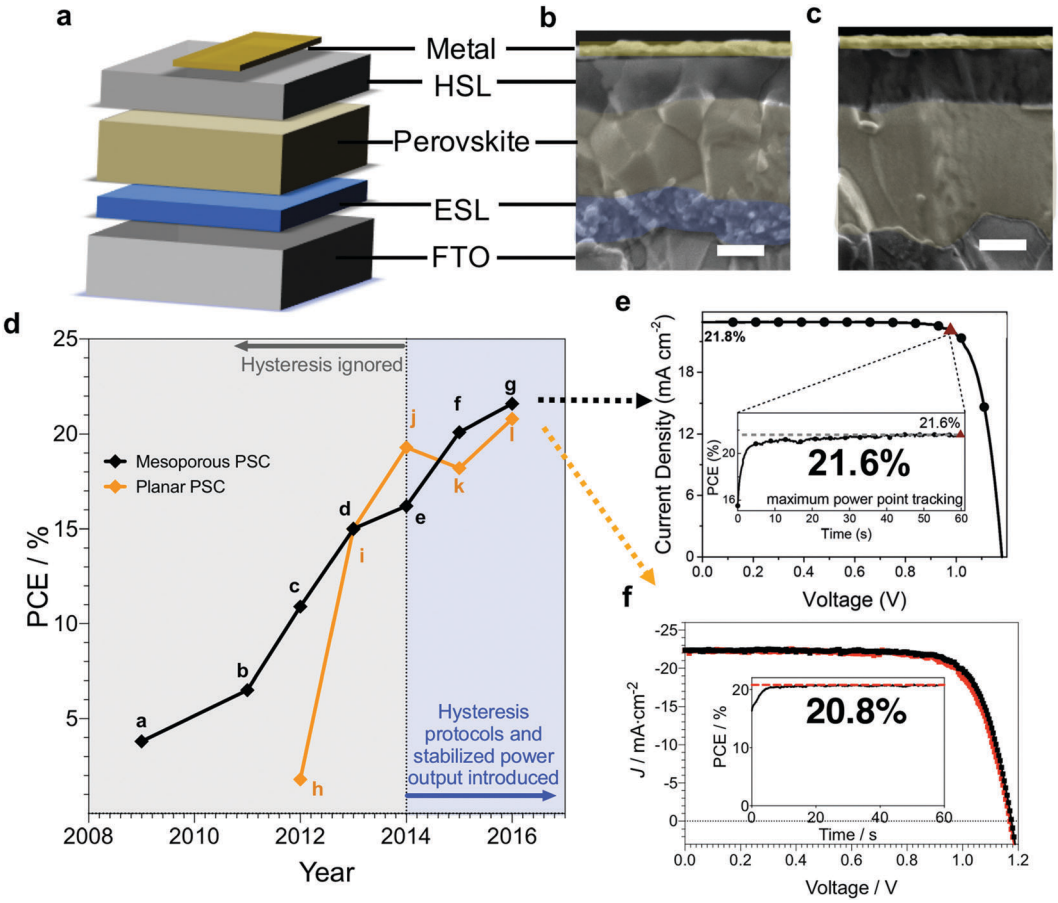

Fig. 4 Evolution of highly efficient PSCs. (a) Schematic of a PSC stack composed of fluorine-doped tin oxide (FTO), a electron transport/selective layer (ESL; typically TiO_2 or SnO_2), Cs/MA/FA/Pb/I/Br perovskite, topped by a hole selective layer (HSL; typically Spiro OMeTAD or PTAA) and a metal electrode. (b) Cross-sectional scanning electron micrograph of a thin mesoporous TiO_2 infiltrated perovskite device, reprinted with permission,[106] and (c) planar atomic layer deposited SnO_2 junction, reprinted with permission.[3] (d) Power conversion efficiency of PSCs over the years. a = ref. 1; b = ref. 107; c = ref. 108; d = ref. 109; e = ref. 110; f = ref. 111; g = ref. 63; h = ref. 108; i = ref. 112; j = ref. 113; k = ref. 3; l = ref. 4. (e) Current–voltage and maximum power point tracking characteristics of the highest published efficiency for a TiO_2 mesoporous infiltrated, reprinted with permission,[63] and (f) a planar SnO_2 heterojunction, reprinted with permission.[4]

improve measuring protocols, and nowadays slow scan rates of the *J–V* hysteresis curve and/or maximum power point tracking are defining the record efficiencies. The first certified PCE was reported by Burschka and coworkers in 2013[109] for a sequential deposition technique where PbI_2 was spin-coated on the TiO_2 mesoporous scaffold and dipped in an MAI solution to form the perovskite material. All subsequent PSC efficiency records have been achieved using a thin (~200 nm) TiO_2 mesoporous layer.

In 2014, a certified 16.2% was achieved by the Seok group and reported in the work of Jeon and coworkers[82] by depositing $MAPbI_3$ films on a 200 nm TiO_2 mesoporous layer, using the so-called "antisolvent" method where a solution of PbI_2 and MAI in a polar solvent is quenched by a non-polar solvent such as toluene during spin coating. This has become the preferred method of deposition and has yielded all the subsequent efficiency records. Another set of breakthroughs by the same group were reported in the works by Jeon *et al.*[56] and Yang *et al.*,[111] yielding 18.5% and 20.1% certified efficiencies, respectively, in 2015. The improved V_{OC} values by the FA/MA Pb-based I/Br perovskites (bandgap *ca.* 1.6 eV) provided the edge for achieving this high performance. A certified 21.0% efficiency was reported in late 2015 by NREL's table of record efficiencies,[114] and recently published by Bi and coworkers[116] using a polymer-templated crystal growth technique of similar cationic/halide mixtures as reported earlier by the Grätzel and Hagfeldt groups yielding efficiencies above 20%.[36,55,117,118] Incorporation of inorganic cations[59–63] became an obvious avenue to improve the crystallographic properties of perovskite materials containing FA and MA mixtures. Two additional efficiency records have been reported by multiple cation formulations including the triple cation incorporating Cs into FA/MA perovskites with a stabilized efficiency of 21.1%, and more recently a quadruple perovskite incorporating Rb into the Cs/FA/MA perovskite mixture with a stabilized efficiency of 21.6% (Fig. 4e). In addition, remarkable V_{oc} values up to 1.24 V for a theoretical maximum of 1.35 V were reported (inset in Fig. 4e).[63] A certified efficiency of 22.1% by the KRICT/UNIST has been reported by NREL, but, at the time of writing, no published reports on the details were found. The chase for efficiency has been a rather hurried and intense one, as can be

seen from the chart in Fig. 4d, for the community though, it has been a very rewarding few years.

Planar junction devices and electron selective layers

The brief history of planar PSCs, where a mesoporous-free device configuration is used, starts with the work of Lee and coworkers[108] in 2012 where, for the first time, a working planar device was published. In that work perovskite was identified to act as both a light absorber and a charge transporter, which was shown by the use of an inert mesoporous scaffold. However, for fully planar devices, an efficiency of 1.8% was reported, which lagged behind the 10.9% mesoporous infiltrated analogue. A large improvement was shown by the same group and shown by Liu *et al.* in 2013, where conformal, evaporated perovskite films were deposited in a planar configuration yielding an efficiency of 15%. As explained earlier, no hysteresis or stabilized power output was shown in this work. Zhou and coworkers published an efficiency of 19.3% without showing hysteresis for that curve in a planar configuration, by doping of the TiO_2 ESL. However, hysteresis is presented in the supporting file of that work with 17% in the backward *vs.* 13% in forward scans, making the efficiency statement blurry. The result came at the time of transition when measuring protocols were not fully established and thus these results must be taken with a grain of salt. Nonetheless, subsequent years showed that high-stabilized efficiencies are possible through modification of the energetics. Correa-Baena *et al.* showed in 2015 that using SnO_2 by ALD (15 nm) and a mixed ion perovskite yielded a stabilized efficiency of 18.2%. In 2016, the use of SnO_2 in the "inverted" PSC configuration also yielded a stabilized efficiency of 18.8%.[104] The use of ionic liquid to control the perovskite morphology yielded a stabilized efficiency of 19.5% using a SnO_2 ESL by ALD in a "traditional" PSC configuration.[119] Energetic modification of TiO_2 by ionic liquids yielded a certified efficiency of 19.4%.[120] More recently, solution-processed SnO_2 ESLs fabricated at low temperature were shown to yield the highest reported stabilized efficiency of 20.8% with V_{OC} values above 1.2 V.[4] Although most of the groups working on improving the efficiency of PSCs have focused on the mesoporous architecture, planar PSCs have made large progress in reaching values above 20%. Some work remains to improve efficiencies beyond the 21% mark.

Hole transport/selective layers: their influence on efficiency and long-term stability

Regardless of the device architecture, the HSL is one of the key components to prepare highly efficient and stable PSCs. We can identify 4 large families of HSLs: small molecule, polymeric, carbon, and inorganic. In this section we will give an overview on the main advantages/disadvantages for each family of HSLs, reporting the most representative recent results.

There are currently hundreds of p-type semiconductor molecules, which have been listed with their corresponding device performance in several recent reviews.[121–125] Small molecules offer the advantage of flexible processing from solution and evaporation, which are compatible with pre-existing industrial lines designed for large-output production of organic electronics. Small molecule optoelectronic properties, in particular the redox potential and the band gap, are relatively easy to modify in order to adjust the molecular backbone to the particular perovskite.[126] The most effective small molecule HSLs to date are spiro-based triphenylamine derivatives.[117] These molecular backbones have a relatively low tendency to crystallize, which enables depositing amorphous organic layers conformally and thus with a good electronic contact to the perovskite surface.[127] Chemical doping of the small molecule HSLs is an essential step to prepare highly efficient PSCs. Lithium salts, organic Lewis bases, and metal–organic oxidants comprise the doping cocktail commonly in use for HSLs in PSCs. The combination and the role of each doping component are more a result of empirical optimizations rather than the application of a thorough design. Increasing hole transporting capabilities (conductivity) while maintaining a low charge recombination at the interface with the perovskite is the most evident effect so far observed by doping the HSLs.[128,129]

Polymeric HSLs have been demonstrated as valid organic alternatives to small molecules. As for the small molecules, triphenylamine is also the most explored unit to prepare highly efficient PSCs.[130] Polymers offer an intrinsic higher hole mobility and lower tendency to crystallize than their small molecule analogues. Extremely thin (10 nm) polymeric HSLs have been demonstrated to be effective for achieving a uniform coating of the perovskite film surface, whereas small molecules are needed above 100 nm thick layers to avoid pinholes.[56] Polymeric ESLs have been exploited as bottom and top selective contacts in solution-processed PSCs, while small molecule ESLs are usually processed as top contacts given the fact that they are relatively less stable to solvent exposure. Despite these advantages, the impact of impurities and batch to batch variation in the polymer synthesis has to be considered for large scale applications of polymeric HSLs in PSCs. More recently, a polymeric HSL, PTAA, was used successfully at high temperatures (85 °C) in a device, rendering remarkable stability under full illumination and maximum power point tracking (MPP).[63]

Carbon HSLs based on nanotubes and nanopowders have been shown as stable alternatives to the organics.[131–134] Carbon nanotube HSLs have been used to prepare highly efficient PSCs, but they may require expensive purification procedures to isolate the right semiconductor tubes.[135] The highest reported efficiency for a carbon nanotube, metal-free device, is 15.5%.[136] Nanopowders offer one of the most economical HSL solutions, which is compatible with the large-scale production lines. However highly efficient PSCs prepared with nanopowder HSLs are still lacking.

Inorganic HSLs have been explored as alternatives for long-term stability, even though device efficiency is still significantly lower, and therefore these layers do not present real advantages over the higher efficiencies by polymeric HSLs.[103] Solution-processed copper thiocyanate is one of the most explored and better performing systems.[137] The deposition of inorganic HSLs as top contacts is complicated as the solvents used in processing tend to be detrimental to the underlying perovskite layer. Bottom contact application or vacuum deposition methods are more

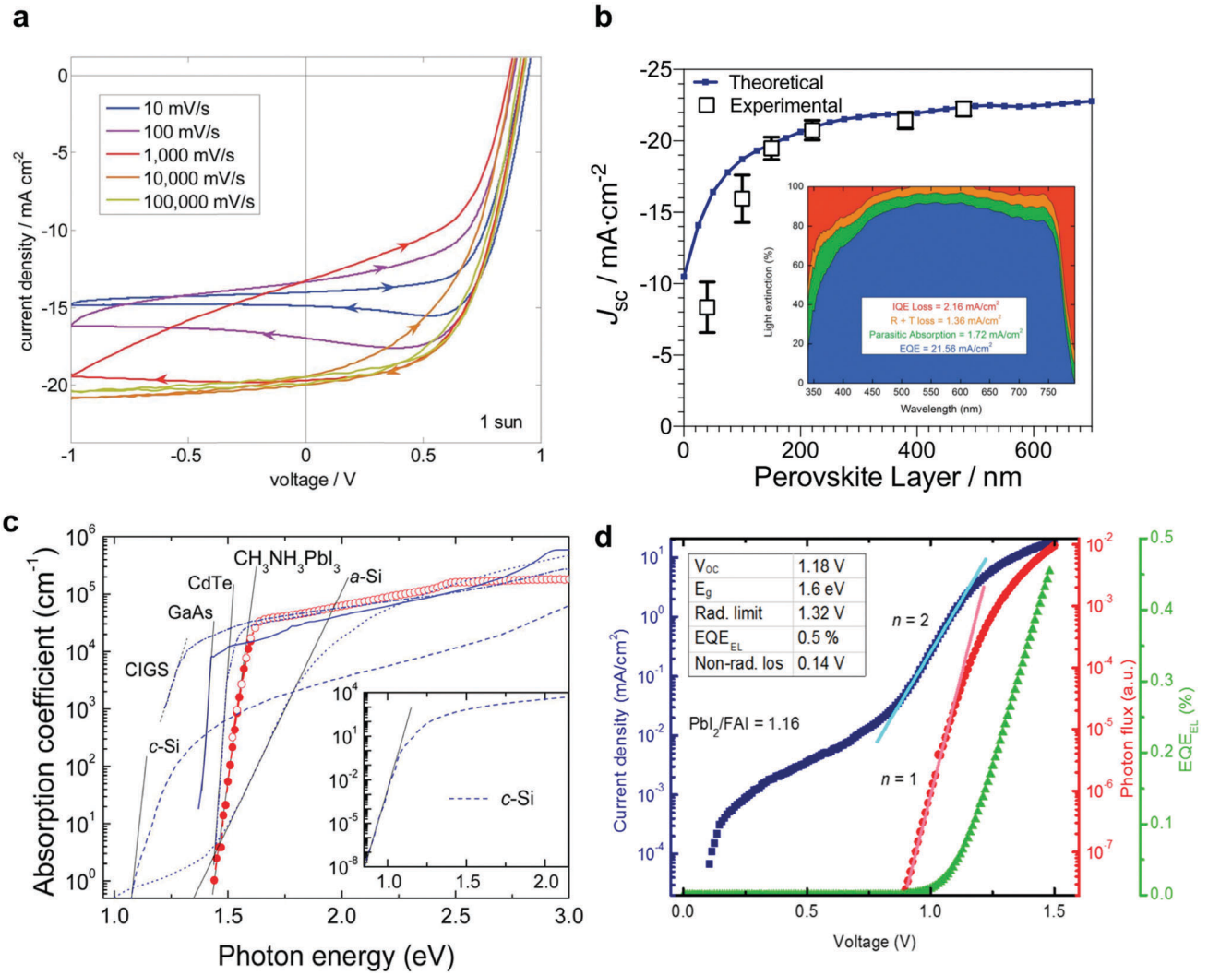

Fig. 5 Perovskite solar cell operational principles. (a) Rate dependent *JV* hysteresis of PSCs, reprinted with permission.[12] (b) Theoretical *vs.* experimental photocurrents as a function of perovskite layer thickness, reprinted with permission.[118] Inset: Parasitic absorption with the calculated photocurrent losses, reprinted with permission.[138] (c) Absorption coefficient of various photovoltaic materials, reprinted with permission.[139] (d) External quantum efficiency of electroluminescence, emission spectrum and dark current of a perovskite solar cell, reprinted with permission.[55]

suitable for inorganics, but they offer less flexibility compared to the organic HSLs.

4. PSC operational principles

Current–voltage hysteresis

Performance parameters in perovskite solar cells cannot be discussed without addressing the hysteresis phenomenon (Fig. 5a): scanning the *JV* curve of perovskite solar cells from positive to negative voltage and *vice versa* results in two different traces. This phenomenon makes the extraction of a power-conversion efficiency from the maximum power point of the *JV* curve ambiguous. After its first reports,[9,140] it became the subject of further investigations, showing that it is a transient phenomenon[10,141] and therefore strongly dependent on the scan rate.[12] It was found that whether hysteresis can be observed under normal measurement conditions depends on the contacts, where inverted PCBM based devices are less prone to hysteresis.[142] Interfacial layer engineering turned out to be crucial to reduce hysteresis.[3] On the other hand, many theoretical and experimental studies indicate that the perovskite itself is responsible for the processes occurring on the timescales of seconds and larger. Consensus has been reached that the migration of ionic defects (such as iodine vacancies) in the perovskite is the most likely underlying process.[12,87,143–146] However, microscopy details and rational control are still lacking and under investigation. In particular, how pronounced the hysteresis is does not only depend on the slow process itself but also on its effect on photogenerated electrons and holes by modifying the recombination and charge extraction probabilities. Recently, even an inverted hysteresis has been reported showing that the hysteresis is a result of complex processes.[11]

Photocurrent density

Analyzing the device structure of the PSC stack is very important to understand the factors that limit the photocurrents. The devices must minimize parasitic losses while the photoabsorber should be grown at an appropriate thickness to capture all photons passing through. Early studies showed photocurrents ranging from 11 mA cm^{-2} for the first PSC liquid prototypes[1] to 18 mA cm^{-2} for the solid state analogues in 2012.[108,115,147] These numbers rapidly increased to above 21 in 2013[112] and above 22 mA cm^{-2} in 2015[56] for PSCs using perovskite materials with a bandgap of around 1.6 eV. Recent work has focused on trying to understand the practical limitations of photocurrent given the device architectures commonly used. Ball *et al.* showed that the main photocurrent losses associated with the device stack come from the internal quantum efficiency (IQE), reflection/transmission losses and parasitic absorption by the FTO/TiO_2/Spiro/Au layers as seen in the inset of Fig. 5b.[138] Work by Correa-Baena and coworkers, exhibited in Fig. 5b, showed that IQE losses are minimized by morphological improvements of the perovskite material, yielding photocurrents that match the theoretical model limitations (where IQE is assumed to be 100%) of around 23 mA cm^{-2}.[118] Here, the perovskite crystal size plays a major role, yielding low and high IQE (close to 100%), for small (40–100 nm) and large crystallites (>150 nm), respectively. Narrowing the bandgap by alloying with Sn perovskites to increase the photocurrents yielded photocurrents of 25 mA cm^{-2},[72,73] and more recently up to 26.9 mA cm^{-2}.[71] Additional work is needed to achieve the theoretical photocurrents for these alloys, as these materials suffer from environmental instability, which hampers their quantum efficiencies.

Open-circuit voltage

When tuning the band gap, the open-circuit voltage (V_{oc}) is influenced as well. For reaching the Shockley–Queisser efficiency limit, V_{oc} needs to approach its thermodynamic limit. This limit is 1.33 V for MAPI (band gap $\approx$1.6 eV) and given by radiative recombination this is not avoidable due to the reciprocity between absorption and emission.[148,149] Broad absorption onsets reduce the maximum V_{oc} without contributing significantly to J_{sc}. Therefore, a sharp absorption onset with a low density of subgap states (Urbach tail) as shown by many perovskite materials is beneficial for high performance (Fig. 5c).[139] Any further loss is due to non-radiative recombination, which can be quantified by measuring the electroluminescence (EL) yield of the solar cell. Once it was possible to make pinhole-free films, the V_{oc} of MAPI devices exceeded 1 V.[99,109,112] Band edge EL spectra were observed with yields in the range of 0.01%.[148,149] Absorption and emission were characteristic of the perovskite instead of any of the other device layers. This and the latest realization of solar cells without any charge transport layers[147,150] made clear that the perovskite itself is the source of the photovoltage generated by a splitting of the quasi-Fermi levels under illumination. Charge transport layers play the role of selective contacts, and non-perfect selectivity results in a decrease of V_{oc} due to surface recombination.[151] Designing more conformal selective layers[3] and optimizing the film morphology and the perovskite composition lead to voltages of $\geq$1.2 V,[55,63,97] which are extraordinarily high and come with an EL yield of approx. 1% (Fig. 5d). The low non-radiative recombination is attributed to the material being a direct semiconductor, where Auger recombination is weak compared to radiative transitions.[152] More importantly, the perovskite shows a pronounced defect tolerance due to the uncommon antibonding nature of the valence band.[153,154] Intrinsic defects (such as vacancies and grain boundaries) causing dangling bonds hardly create deep trap states in the band gap which would act as efficient recombination centers as shown by DFT calculations.[76,155] Consequently, the reported highest-voltage solar cells do not demand any specific passivation measures. Nevertheless, a further increase of V_{oc} requires understanding and exclusion of extrinsic sources of recombination such as impurities and interfaces.

Fill factor

The fill factor (FF) is linked to V_{oc} *via* recombination resulting in maximum values of state-of-the-art devices of approx. 82%.[151] Lower values are caused by additional losses due to charge extraction that depends on the electric field, and thus on voltage, external series resistances or shunt paths. Despite the high mobilities and diffusion lengths reported for perovskites,[158–160] which should easily allow the recombination limit of the FF to be reached in a film of a few 100 nm thickness, often the FF is lower. This can be due to charge extraction into resistive charge selective layers[4,128] or due to the perovskite itself. Whereas grain boundaries do not seem to strongly affect V_{oc} and thus recombination, they reduce the FF, even resulting in an anti-correlation of the FF and the thickness (Fig. 6a).[118] This indicates that grain boundaries constitute an obstacle for charge transport. Inverted devices have shown the highest values of FF (however at voltages <1 V) so far[156,161] peaking at 85% for a device with 2% Sr (in solution) added in $MAPbI_3$ (Fig. 6b).[156] Increasing the FF further and approaching its theoretical limit of 91% (for $MAPbI_3$), needs to occur along with increasing the V_{oc}, and will likely be the subject of future work by the PSC community.

The role of the energetics of adjacent layers

The band structure of perovskite materials for applications in PSCs has shown several facets, and understanding these is very important for maximizing both efficiency and stability. First, in contrast to early hypotheses,[162] it is unlikely that the ionization energies at the interfaces, obtained by ultraviolet photoelectron spectroscopy (UPS) for the adjacent charge transport layers, are necessarily the determining factors for the design of high V_{OC} and thus high efficiency PSCs. This is due to 2 reasons: (i) notorious ionic movement within or at the surface of the perovskite material under working conditions has been shown to change its energetics[3,11,163,164] and (ii) ionization potentials have been shown to vary tremendously with the deposition technique or stoichiometry of the precursors as seen in Fig. 6c,[157] and with the substrates used for perovskite deposition.[165] Therefore, small changes in composition or biasing of the

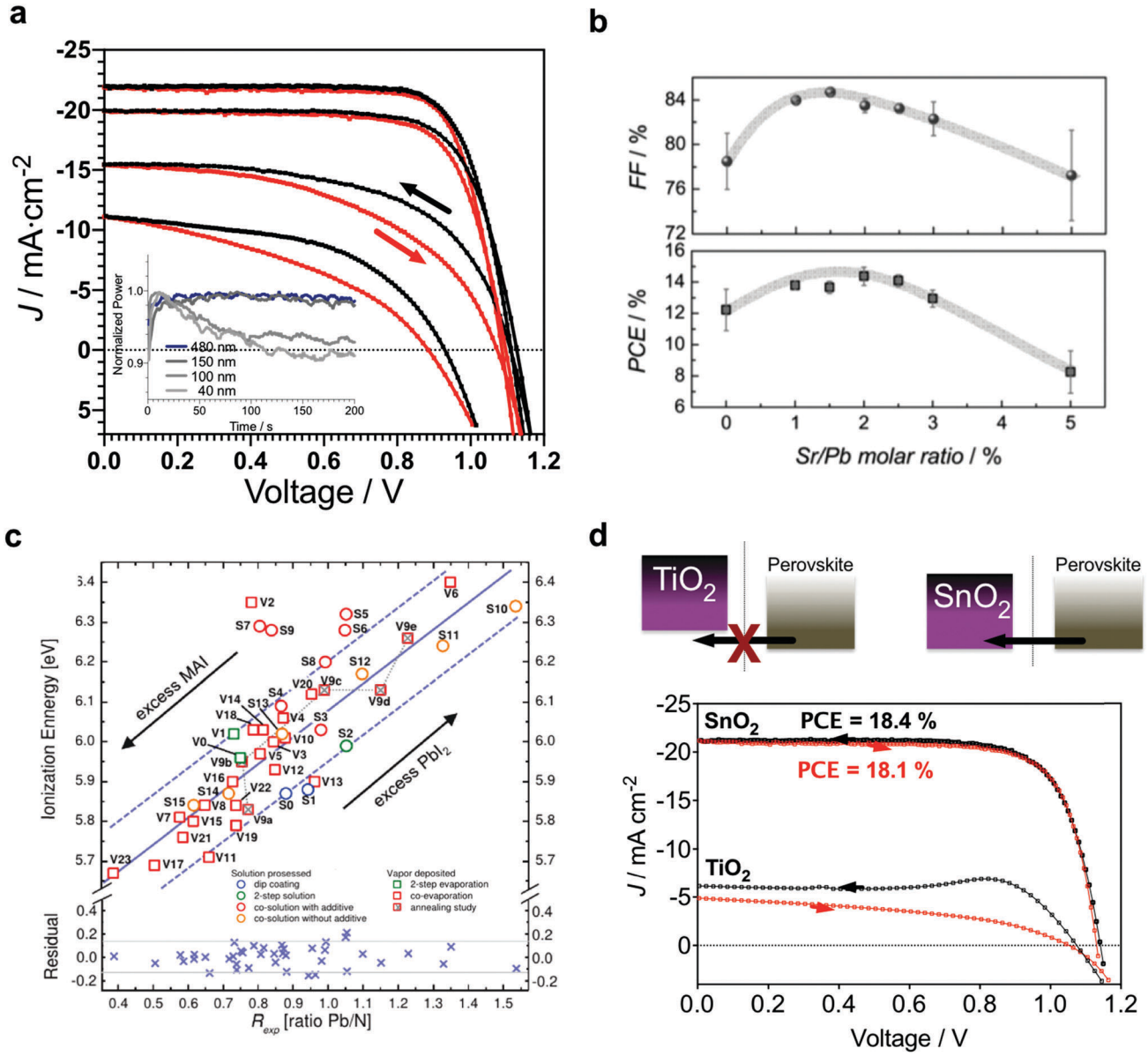

Fig. 6 Fill factor and energetics of PSCs. (a) J–V curves (10 mV s^{-1}) of PSCs with different thicknesses/crystal sizes, reprinted with permission.[118] (b) Fill factor and power conversion efficiency as a function of Sr^{2+} incorporation into $MAPbI_3$ devices, reprinted with permission.[156] (c) Ionization energy *vs.* perovskite composition and deposition technique, reprinted with permission.[157] (d) Schematic of an energetic barrier in PSCs and the corresponding current–voltage curves for atomic layer deposited TiO_2 and SnO_2, reprinted with permission.[3]

device can yield dramatic differences in the ionization energy, making it difficult to have a general rule or understanding for these interfaces. What seems to be more certain is that the band edges of the charge transport layers do not necessarily determine the open circuit voltage of the device. The valence band, or highest occupied molecular orbital, energy position of the HTL has been shown to have no effect on the voltage of iodine[166,167] or bromine-based[168] perovskite materials. On the other hand, energetic barriers, on both the ETL[3] and the HTL,[166] have been shown to create injection issues, which in turn yield low photocurrents (Fig. 6d), or hysteretic J–V curves.[3,11] Therefore, as long as there is no energetic barrier, tuning of the work function of the charge selective layers seems to be unnecessary when designing PSCs for high V_{OC} and high efficiency.

Testing procedures

Measurement procedures for the initial and long-term power conversion efficiency of perovskite solar cells demand an adjustment of standard protocols in use for other photovoltaic devices due to the current–voltage hysteresis. Therefore, before considering the long-term stability measurements of PSCs, a robust method for measuring performance is needed. The J–V characteristic is normally used to extract the solar cell performance parameters, such as J_{sc}, V_{oc}, and the fill factor (FF) and to determine the MPP and in turn the power-conversion

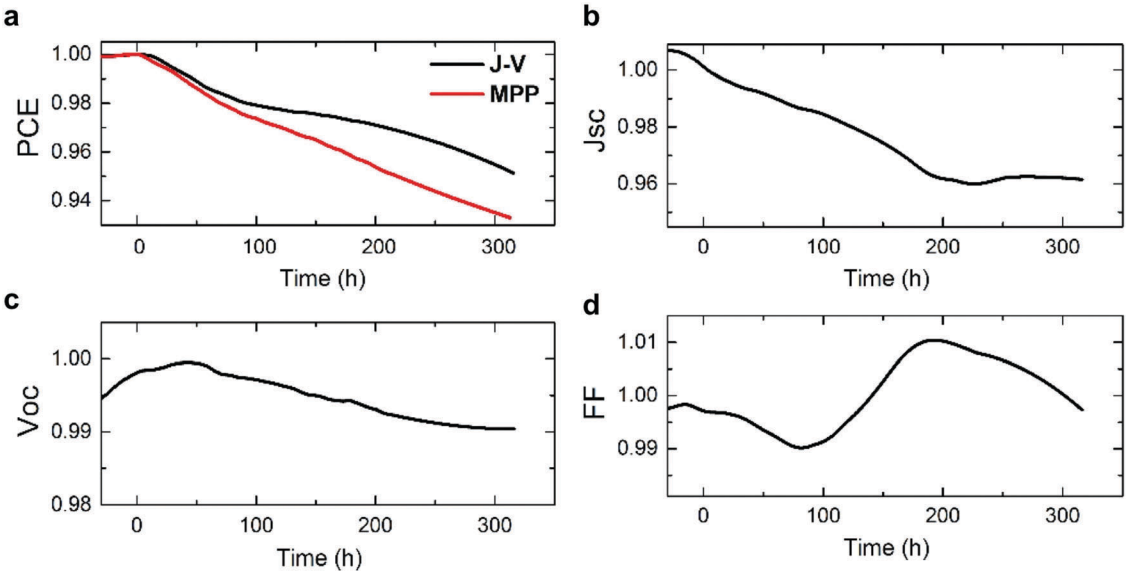

Fig. 7 Testing protocols for PSCs. Maximum power conversion efficiency (PCE) as a function of the time extracted from the *J–V* (backward scan 100 mV s^{-1}) and from the MPP tracking of a single device. Device performance parameters (J_{sc}, V_{oc} and FF) were extracted from the *J–V* characteristics collected every hour. The device was continuously operated at the MPP except during the *J–V* measurement. All the data are normalized to the maximum value. Data are reported in the ESI in the study of Saliba *et al.*, modified with permission.[72]

efficiency. In perovskite solar cells, the *J–V* curve is a necessary but not sufficient test to estimate the actual maximum power. Indeed, the occurrence of the hysteresis complicates the collection of a stabilized *J–V* curve, which results in an MPP that depends on the testing conditions such as prebiasing, scan rate, and light soaking. Tracking the MPP using a perturb-and-observe method is a common practical solution to estimate a stabilized value and therefore to calculate the actual device maximum power conversion efficiency (PCE). Depending on testing and ageing conditions, a *J–V* curve can significantly overestimate the actual device PCE. Fig. 7 displays the PCE as a function of time for a single device recently published by Saliba *et al.*[72] We can observe that the PCE extracted from the *J–V* (backward scan, 100 mV s^{-1}) and the MPP are close at the early stage of the test. As the device ages under light the PCE from the *J–V* becomes significantly larger than that from MPP. As expected from an ageing device, the J_{sc} and the V_{oc} monotonically decrease over time, however the FF shows a more complex trend with an unexpected improvement. As observed by Tress *et al.*, the occurrence of this behaviour is an artefact resulting from the hysteresis becoming more severe with the device ageing.[12] Therefore the MPP tracking is an essential test to draw conclusions about the efficiency and long-term stability of the perovskite solar cells, which will be discussed in the next section.

5. Long-term stability of perovskite solar cells

PSCs have been demonstrated to be capable of converting sunlight into electricity with efficiencies comparable to those of conventional thin-film solar cells. Therefore, the next obvious challenge is to make the perovskite as stable as the other materials. The literature on the stability of PSCs is rather complex to read since no uniform ageing test conditions are in use. Even more difficult is that stability data are often extracted from *J–V* curves, which may significantly overestimate the performance in aged devices (see the testing procedures in Section 3). Given this scenario, we cautiously report only results that have been verified from several groups rather than in a single study, using particular testing conditions.

The stability of the PSCs depends on a number of potential degradation factors. Humidity has been demonstrated as the most aggressive cause of performance loss due to the strong interaction with the water molecule as show in Fig. 8a. These so-called extrinsic factors can activate several degradation mechanisms, involving the perovskite and the other materials in the device.[169] However, different encapsulation procedures have been demonstrated to be quite effective in isolating the device from these external sources of degradation as shown in Fig. 8b.[170] More alarming are potential intrinsic instabilities that are active also under inert conditions. These can impact the perovskite and the other materials in the device.

Small molecule HSLs suffer from crystallization at relatively high temperature, which reduces the electronic contact with the perovskite and the metal electrode reducing the device performance as shown in Fig. 5c. Gold has been largely used as a top metal contact to prepare lab-scale PSCs (Fig. 8d). It has been recently shown that gold migration within small molecule HSLs is responsible for rapid performance losses, when tested at moderate temperature (70 °C).[106] This effect then becomes the dominant factor in the performance losses. Therefore, blocking the gold migration is essential to study the stability

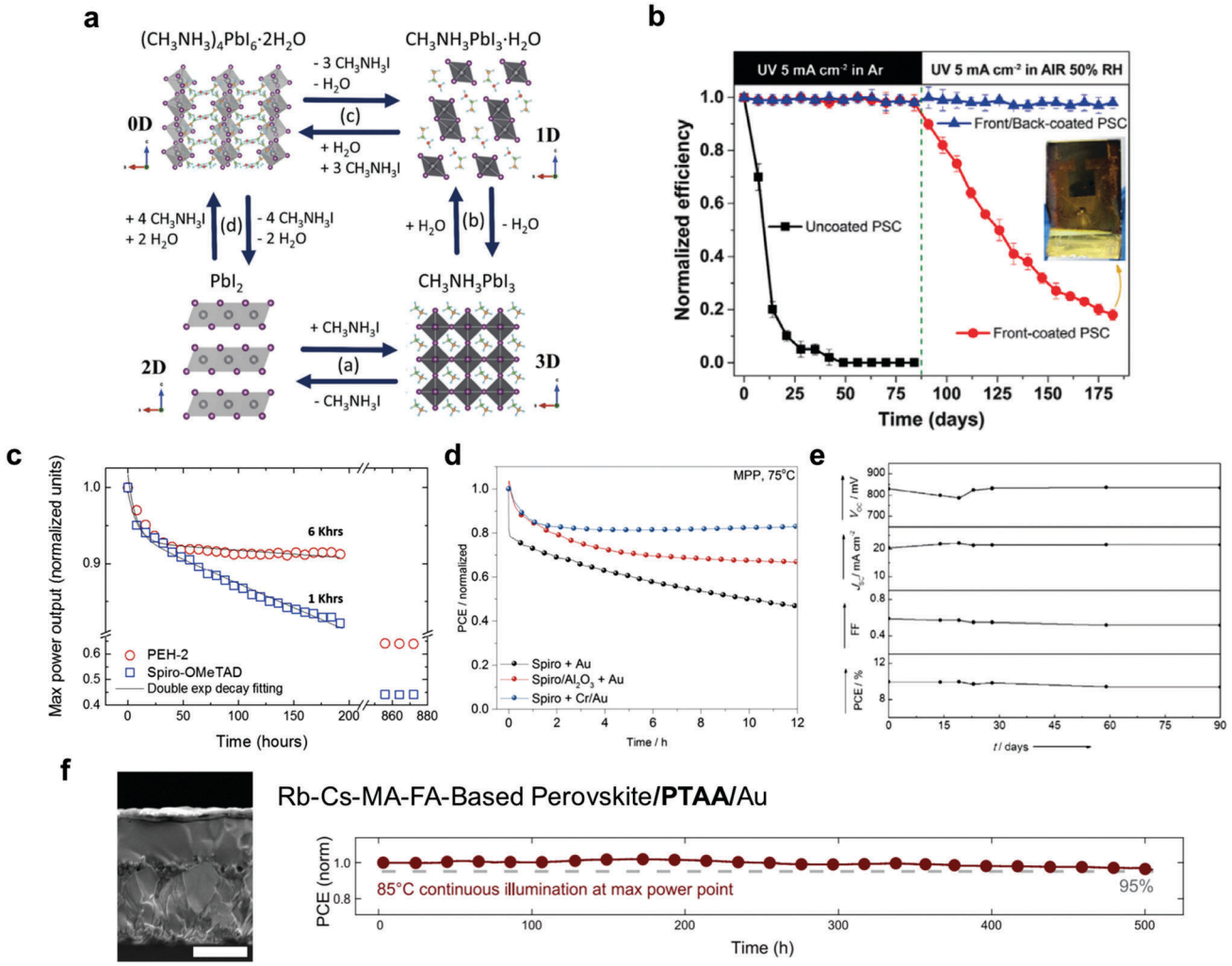

Fig. 8 Mechanisms of perovskite solar cell degradation. (a) Schematic diagram of the interactions of the water molecule with the perovskite material, reprinted with permission.[169] (b) Encapsulation techniques to avoid moisture and UV instability, reprinted with permission.[170] (c) MPPT over time with two different HSLs, reprinted with permission.[171] (d) MPPT of PSCs at 75 °C on a Spiro-based device with different interlayers, reprinted with permission.[106] (e) Current–voltage parameters over time (90 days) using carbon electrodes in outdoor testing under dry and hot (desert) conditions, reprinted with permission.[132] (f) Scanning electron micrograph of PTAA-based devices and the respective MPPT over time (500 hours) at 85 °C and continuous illumination, reprinted with permission.[63]

of small molecule HSLs. Carbon based HSLs offer one of the most stable solutions even though the device efficiency seems to be not yet comparable to the organic HSLs (Fig. 8e).[133] Interestingly, polymeric HSLs demonstrated a good barrier to the gold migration as shown in Fig. 8f,[63] as well as chromium interlayers[106,172] and alumina nanoparticle buffer layers (Fig. 8d).[173] Polymeric HSLs are thermally more stable than small molecules and they have been demonstrated to be stable within the whole operating temperature range of solar cells.[63,174] Metal oxides used as ESLs suffer from the UV-activated degradation mechanism. Reducing the amount of metal oxide or using chemical doping to stabilize the metal oxides has been demonstrated as an effective strategy to improve the UV stability of PSCs.[175,176]

The perovskite layer is the core of the device and its stability is crucial to deliver a PSC technology for commercialization. It is well documented, and has been discussed above, that ionic defects form during the perovskite preparation or during the device operation. These defects do not seem to be particularly detrimental within the bulk of the perovskite layer, since they induce donor and acceptor electronic states close or within the conduction and valence band, respectively.[155] However, ionic defects can migrate from the bulk to the edge of the perovskite at the interface with the selective contact.[177] Here they can accumulate forming a space charge layer that hampers the charge extraction efficiency. The space charged region may be particularly reactive with the selective contact at the interface. This potential intrinsic instability is still under investigation, however, it seems clear that the interface between the perovskite and the selective contact is playing a role in the device stability. Reducing the number of defects by using mixed perovskite compositions, chemical doping, or surface passivation has

been demonstrated as a valuable strategy to improve the device stability.[178,179]

6. Future outlook

Solution-processed perovskite materials have achieved remarkable milestones in just a few years. They have been used in a myriad of applications from solar cells to light emitting devices and photodetectors. In this review we have outlined and discussed the excellent optoelectronic properties, solar cell physics, and most recent performance and long-term stability improvements of perovskites. This has continued the excitement in the field, but some additional work needs be done to understand and improve further the photovoltaic parameters and long-term stability under working conditions.

Going forward, PSCs will have to reduce non-radiative recombination and improve charge transport in order to achieve the highest possible V_{OC} values and fill factors. The studies described in this review have made considerable advances in both parameters, and additional investigations need to address further improvements to non-radiative recombination and the conductivity of the perovskite/charge selective layers in order to go beyond the efficiency of 22%. Regardless, the impressive advancement in such a small amount of time is unprecedented and we may soon reach crystalline silicon and GaAs records towards the 29% mark.[114] Shockley–Queisser also showed that the open-circuit voltage, V_{oc}, needs to be corrected from the ideal value if the external luminescence is less than 100%. A high external luminescence is thus essential for achieving high voltage from a solar cell. This is the case for GaAs, which can be explained by a photon recycling mechanism in which photons are reabsorbed and re-emitted many times before an electron–hole pair is collected or a luminescent photon escapes. This year Pazos-Outon *et al.*[180] provided evidence that PSCs have an internal photon gas showing photon recycling properties. As mentioned above, remarkably high V_{oc} and external electroluminescence have also been obtained for PSCs. For example, a V_{oc} of 1.24 V was achieved with a band gap perovskite material of 1.64 V.[63] Compared to the theoretical limit of V_{oc} for such a band gap, the difference is only about 100 mV. This is astonishing and already better than all other photovoltaic technologies, including silicon, with the exception of GaAs. Consequently, a high EQE electroluminescence was obtained at 3.8% in the solar cell mode, which outperforms the best silicon solar cells showing an EQE of about 0.5%.[181]

For all the published efficiencies, especially when measuring records, it is important to use maximum power point tracking or stabilized power output, as these values are more representative than hysteresis prone *J–V* curves. To measure long-term stability, most groups have resorted to "dark shelf" testing, but to be representative of more realistic operating conditions, these tests should include maximum power point tracking and 1 sun illumination. In addition, recent work has shown that both humidity and UV illumination have no major effect on the long-term stability, as long as appropriate encapsulation/UV absorbers are applied. A very encouraging result was also reported recently showing a stable efficiency at 85 °C for 500 h under full solar illumination and maximum power point tracking (95% of the initial performance was retained).[63] There are certainly challenges remaining in trying to understand the role of ionic movement in long-term stability, and how to improve the already excellent photovoltaic parameters of PSCs. It is expected, however, that the PSC field will have additional years of exciting new findings which will maintain the interest of both academia and industry.

References

1 A. Kojima, K. Teshima, Y. Shirai and T. Miyasaka, *J. Am. Chem. Soc.*, 2009, **131**, 6050–6051.
2 NREL, Best Research-Cell Efficiencies, http://www.nrel.gov, accessed: November 2016.
3 J. P. Correa Baena, L. Steier, W. Tress, M. Saliba, S. Neutzner, T. Matsui, F. Giordano, T. J. Jacobsson, A. R. Srimath Kandada, S. M. Zakeeruddin, A. Petrozza, A. Abate, M. K. Nazeeruddin, M. Gratzel and A. Hagfeldt, *Energy Environ. Sci.*, 2015, **8**, 2928–2934.
4 E. H. Anaraki, A. Kermanpur, L. Steier, K. Domanski, T. Matsui, W. Tress, M. Saliba, A. Abate, M. Gratzel, A. Hagfeldt and J.-P. Correa-Baena, *Energy Environ. Sci.*, 2016, **9**, 3128–3134.
5 J. Werner, C.-H. Weng, A. Walter, L. Fesquet, J. P. Seif, S. De Wolf, B. Niesen and C. Ballif, *J. Phys. Chem. Lett.*, 2016, **7**, 161–166.
6 S. Albrecht, M. Saliba, J. P. Correa Baena, F. Lang, L. Kegelmann, M. Mews, L. Steier, A. Abate, J. Rappich, L. Korte, R. Schlatmann, M. K. Nazeeruddin, A. Hagfeldt, M. Gratzel and B. Rech, *Energy Environ. Sci.*, 2016, **9**, 81–88.
7 X. Li, D. Bi, C. Yi, J.-D. Décoppet, J. Luo, S. M. Zakeeruddin, A. Hagfeldt and M. Grätzel, *Science*, 2016, **353**, 58–62.
8 J. A. Christians, J. S. Manser and P. V. Kamat, *J. Phys. Chem. Lett.*, 2015, **6**, 852–857.
9 H. J. Snaith, A. Abate, J. M. Ball, G. E. Eperon, T. Leijtens, N. K. Noel, S. D. Stranks, J. T.-W. Wang, K. Wojciechowski and W. Zhang, *J. Phys. Chem. Lett.*, 2014, **5**, 1511–1515.
10 E. L. Unger, E. T. Hoke, C. D. Bailie, W. H. Nguyen, A. R. Bowring, T. Heumuller, M. G. Christoforo and M. D. McGehee, *Energy Environ. Sci.*, 2014, **7**, 3690–3698.
11 W. Tress, J. P. Correa Baena, M. Saliba, A. Abate and M. Graetzel, *Adv. Energy Mater.*, 2016, **6**, 1600396.
12 W. Tress, N. Marinova, T. Moehl, S. M. Zakeeruddin, M. K. Nazeeruddin and M. Gratzel, *Energy Environ. Sci.*, 2015, **8**, 995–1004.
13 K. Domanski, B. Roose, T. Matsui, M. Saliba, S.-H. Turren-Cruz, J.-P. Correa-Baena, C. R. Carmona, G. Richardson, J. M. Foster, F. De Angelis, J. M. Ball, A. Petrozza, N. Mine, M. K. Nazeeruddin, W. Tress, M. Gratzel, U. Steiner, A. Hagfeldt and A. Abate, *Energy Environ. Sci.*, 2017, DOI: 10.1039/C6EE03352K.
14 V. M. Goldschmidt, *Naturwissenschaften*, 1926, **14**, 477–485.

15 D. B. Mitzi, S. Wang, C. A. Feild, C. A. Chess and A. M. Guloy, *Science*, 1995, **267**, 1473–1476.
16 J. Calabrese, N. L. Jones, R. L. Harlow, N. Herron, D. L. Thorn and Y. Wang, *J. Am. Chem. Soc.*, 1991, **113**, 2328–2330.
17 S. M. Wang, D. B. Mitzi, C. A. Feild and A. Guloy, *J. Am. Chem. Soc.*, 1995, **117**, 5297–5302.
18 B. Saparov and D. B. Mitzi, *Chem. Rev.*, 2016, **116**, 4558–4596.
19 H. G. Kim, O. S. Becker, J. S. Jang, S. M. Ji, P. H. Borse and J. S. Lee, *J. Solid State Chem.*, 2006, **179**, 1214–1218.
20 H. Tsai, W. Nie, J.-C. Blancon, C. C. Stoumpos, R. Asadpour, B. Harutyunyan, A. J. Neukirch, R. Verduzco, J. J. Crochet, S. Tretiak, L. Pedesseau, J. Even, M. A. Alam, G. Gupta, J. Lou, P. M. Ajayan, M. J. Bedzyk, M. G. Kanatzidis and A. D. Mohite, *Nature*, 2016, **536**, 312–316.
21 I. C. Smith, E. T. Hoke, D. Solis-Ibarra, M. D. McGehee and H. I. Karunadasa, *Angew. Chem.*, 2014, **126**, 11414–11417.
22 N. K. McKinnon, D. C. Reeves and M. H. Akabas, *J. Gen. Physiol.*, 2011, **138**, 453–466.
23 Y. Y. Dang, Y. Liu, Y. X. Sun, D. S. Yuan, X. L. Liu, W. Q. Lu, G. F. Liu, H. B. Xia and X. T. Tao, *CrystEngComm*, 2015, **17**, 665–670.
24 N. Onodayamamuro, T. Matsuo and H. Suga, *J. Phys. Chem. Solids*, 1992, **53**, 935–939.
25 V. D'Innocenzo, G. Grancini, M. J. P. Alcocer, A. R. S. Kandada, S. D. Stranks, M. M. Lee, G. Lanzani, H. J. Snaith and A. Petrozza, *Nat. Commun.*, 2014, **5**, 3586.
26 H. Wang, L. Whittaker-Brooks and G. R. Fleming, *J. Phys. Chem. C*, 2015, **119**, 19590–19595.
27 T. Baikie, Y. N. Fang, J. M. Kadro, M. Schreyer, F. X. Wei, S. G. Mhaisalkar, M. Graetzel and T. J. White, *J. Mater. Chem. A*, 2013, **1**, 5628–5641.
28 T. J. Jacobsson, W. Tress, J. P. Correa-Baena, T. Edvinsson and A. Hagfeldt, *J. Phys. Chem. C*, 2016, **120**, 11382–11393.
29 C. C. Stoumpos, C. D. Malliakas and M. G. Kanatzidis, *Inorg. Chem.*, 2013, **52**, 9019–9038.
30 T. J. Jacobsson, L. J. Schwan, M. Ottosson, A. Hagfeldt and T. Edvinsson, *Inorg. Chem.*, 2015, **54**, 10678–10685.
31 A. Poglitsch and D. Weber, *J. Chem. Phys.*, 1987, **87**, 6373–6378.
32 C. Quarti, E. Mosconi, J. M. Ball, V. D'Innocenzo, C. Tao, S. Pathak, H. J. Snaith, A. Petrozza and F. De Angelis, *Energy Environ. Sci.*, 2016, **9**, 155–163.
33 M. I. Saidaminov, A. L. Abdelhady, G. Maculan and O. M. Bakr, *Chem. Commun.*, 2015, **51**, 17658–17661.
34 J. Su, D. P. Chen and C. T. Lin, *J. Cryst. Growth*, 2015, **422**, 75–79.
35 S. Yakunin, L. Protesescu, F. Krieg, M. I. Bodnarchuk, G. Nedelcu, M. Humer, G. De Luca, M. Fiebig, W. Heiss and M. V. Kovalenko, *Nat. Commun.*, 2015, **6**, 8056.
36 T. Jesper Jacobsson, J.-P. Correa-Baena, M. Pazoki, M. Saliba, K. Schenk, M. Gratzel and A. Hagfeldt, *Energy Environ. Sci.*, 2016, **9**, 1706–1724.
37 D. M. Jang, K. Park, D. H. Kim, J. Park, F. Shojaei, H. S. Kang, J. P. Ahn, J. W. Lee and J. K. Song, *Nano Lett.*, 2015, **15**, 5191–5199.
38 A. Sadhanala, S. Ahmad, B. D. Zhao, N. Giesbrecht, P. M. Pearce, F. Deschler, R. L. Z. Hoye, K. C. Godel, T. Bein, P. Docampo, S. E. Dutton, M. F. L. De Volder and R. H. Friend, *Nano Lett.*, 2015, **15**, 6095–6101.
39 Y. C. Liu, Z. Yang, D. Cui, X. D. Ren, J. K. Sun, X. J. Liu, J. R. Zhang, Q. B. Wei, H. B. Fan, F. Y. Yu, X. Zhang, C. M. Zhao and S. Z. Liu, *Adv. Mater.*, 2015, **27**, 5176–5183.
40 Q. Dong, Y. Fang, Y. Shao, P. Mulligan, J. Qiu, L. Cao and J. Huang, *Science*, 2015, **347**, 967–970.
41 D. Shi, V. Adinolfi, R. Comin, M. J. Yuan, E. Alarousu, A. Buin, Y. Chen, S. Hoogland, A. Rothenberger, K. Katsiev, Y. Losovyj, X. Zhang, P. A. Dowben, O. F. Mohammed, E. H. Sargent and O. M. Bakr, *Science*, 2015, **347**, 519–522.
42 A. Maaej, M. Bahri, Y. Abid, N. Jaidane, Z. B. Lakhdar and A. Lautie, *Phase Transitions*, 1998, **64**, 179–190.
43 J. W. Lee, D. J. Seol, A. N. Cho and N. G. Park, *Adv. Mater.*, 2014, **26**, 4991–4998.
44 W. S. Yang, J. H. Noh, N. J. Jeon, Y. C. Kim, S. Ryu, J. Seo and S. I. Seok, *Science*, 2015, **348**, 1234–1237.
45 M. Pazoki, T. J. Jacobsson, A. Hagfeldt, G. Boschloo and T. Edvinsson, *Phys. Rev. B: Condens. Matter Mater. Phys.*, 2016, **93**, 4105.
46 T. J. Jacobsson, M. Pazoki, A. Hagfeldt and T. Edvinsson, *J. Phys. Chem. C*, 2015, **119**, 25673–25683.
47 M. R. Filip, G. E. Eperon, H. J. Snaith and F. Giustino, *Nat. Commun.*, 2014, **5**, 1.
48 M. T. Weller, O. J. Weber, J. M. Frost and A. Walsh, *J. Phys. Chem. Lett.*, 2015, **6**, 3209–3212.
49 S. Pang, H. Hu, J. Zhang, S. Lv, Y. Yu, F. Wei, T. Qin, H. Xu, Z. Liu and G. Cui, *Chem. Mater.*, 2014, **26**, 1485–1491.
50 A. Binek, F. C. Hanusch, P. Docampo and T. Bein, *J. Phys. Chem. Lett.*, 2015, **6**, 1249–1253.
51 T. M. Koh, K. Fu, Y. Fang, S. Chen, T. C. Sum, N. Mathews, S. G. Mhaisalkar, P. P. Boix and T. Baikie, *J. Phys. Chem. C*, 2014, **118**, 16458–16462.
52 F. C. Hanusch, E. Wiesenmayer, E. Mankel, A. Binek, P. Angloher, C. Fraunhofer, N. Giesbrecht, J. M. Feckl, W. Jaegermann, D. Johrendt, T. Bein and P. Docampo, *J. Phys. Chem. Lett.*, 2014, **5**, 2791–2795.
53 C. Roldan-Carmona, P. Gratia, I. Zimmermann, G. Grancini, P. Gao, M. Graetzel and M. K. Nazeeruddin, *Energy Environ. Sci.*, 2015, **8**, 3550–3556.
54 N. Pellet, P. Gao, G. Gregori, T. Y. Yang, M. K. Nazeeruddin, J. Maier and M. Gratzel, *Angew. Chem., Int. Ed.*, 2014, **53**, 3151–3157.
55 D. Bi, W. Tress, M. I. Dar, P. Gao, J. Luo, C. Renevier, K. Schenk, A. Abate, F. Giordano, J.-P. Correa Baena, J.-D. Decoppet, S. M. Zakeeruddin, M. K. Nazeeruddin, M. Grätzel and A. Hagfeldt, *Sci. Adv.*, 2016, **2**, e1501170.
56 N. J. Jeon, J. H. Noh, W. S. Yang, Y. C. Kim, S. Ryu, J. Seo and S. I. Seok, *Nature*, 2015, **517**, 476–480.
57 F. Brivio, C. Caetano and A. Walsh, *J. Phys. Chem. Lett.*, 2016, **7**, 1083–1087.
58 N. Pellet, P. Gao, G. Gregori, T. Y. Yang, M. K. Nazeeruddin, J. Maier and M. Grätzel, *Angew. Chem., Int. Ed.*, 2014, **53**, 3151–3157.

59 C. Yi, J. Luo, S. Meloni, A. Boziki, N. Ashari-Astani, C. Gratzel, S. M. Zakeeruddin, U. Rothlisberger and M. Gratzel, *Energy Environ. Sci.*, 2016, **9**, 656–662.
60 J.-W. Lee, D.-H. Kim, H.-S. Kim, S.-W. Seo, S. M. Cho and N.-G. Park, *Adv. Energy Mater.*, 2015, **5**, 1501310.
61 D. P. McMeekin, G. Sadoughi, W. Rehman, G. E. Eperon, M. Saliba, M. T. Hörantner, A. Haghighirad, N. Sakai, L. Korte, B. Rech, M. B. Johnston, L. M. Herz and H. J. Snaith, *Science*, 2016, **351**, 151–155.
62 M. Saliba, T. Matsui, J.-Y. Seo, K. Domanski, J.-P. Correa-Baena, M. K. Nazeeruddin, S. M. Zakeeruddin, W. Tress, A. Abate, A. Hagfeldt and M. Gratzel, *Energy Environ. Sci.*, 2016, **9**, 1989–1997.
63 M. Saliba, T. Matsui, K. Domanski, J.-Y. Seo, A. Ummadisingu, S. M. Zakeeruddin, J.-P. Correa-Baena, W. R. Tress, A. Abate, A. Hagfeldt and M. Grätzel, *Science*, 2016, **354**, 206–209.
64 B. W. Park, B. Philippe, X. L. Zhang, H. Rensmo, G. Boschloo and E. M. J. Johansson, *Adv. Mater.*, 2015, **27**, 6806–6813.
65 Y. Y. Sun, J. Shi, J. Lian, W. W. Gao, M. L. Agiorgousis, P. H. Zhang and S. B. Zhang, *Nanoscale*, 2016, **8**, 6284–6289.
66 P. P. Boix, S. Agarwala, T. M. Koh, N. Mathews and S. G. Mhaisalkar, *J. Phys. Chem. Lett.*, 2015, **6**, 898–907.
67 F. Giustino and H. J. Snaith, *ACS Energy Lett.*, 2016, **1**, 1233–1240.
68 N. K. Noel, S. D. Stranks, A. Abate, C. Wehrenfennig, S. Guarnera, A. A. Haghighirad, A. Sadhanala, G. E. Eperon, S. K. Pathak, M. B. Johnston, A. Petrozza, L. M. Herz and H. J. Snaith, *Energy Environ. Sci.*, 2014, **7**, 3061–3068.
69 F. Hao, C. C. Stoumpos, D. H. Cao, R. P. H. Chang and M. G. Kanatzidis, *Nat. Photonics*, 2014, **8**, 489–494.
70 A. Babayigit, A. Ethirajan, M. Muller and B. Conings, *Nat. Mater.*, 2016, **15**, 247–251.
71 W. Liao, D. Zhao, Y. Yu, N. Shrestha, K. Ghimire, C. R. Grice, C. Wang, Y. Xiao, A. J. Cimaroli, R. J. Ellingson, N. J. Podraza, K. Zhu, R.-G. Xiong and Y. Yan, *J. Am. Chem. Soc.*, 2016, **138**, 12360–12363.
72 M. Anaya, J. P. Correa-Baena, G. Lozano, M. Saliba, P. Anguita, B. Roose, A. Abate, U. Steiner, M. Gratzel, M. E. Calvo, A. Hagfeldt and H. Miguez, *J. Mater. Chem. A*, 2016, **4**, 11214–11221.
73 G. E. Eperon, T. Leijtens, K. A. Bush, T. Green, J. Tse-Wei Wang, D. P. McMeekin, G. Volonakis, R. L. Milot, D. J. Slotcavage, R. Belisle, J. B. Patel, E. S. Parrott, R. J. Sutton, W. Ma, F. Moghadam, B. Conings, A. Babayigit, H.-G. Boyen, F. Giustino, L. M. Herz, M. B. Johnston, M. D. McGehee and H. J. Snaith, *Science*, 2016, **354**, 861–865.
74 R. E. Brandt, R. C. Kurchin, R. L. Z. Hoye, J. R. Poindexter, M. W. B. Wilson, S. Sulekar, F. Lenahan, P. X. T. Yen, V. Stevanović, J. C. Nino, M. G. Bawendi and T. Buonassisi, *J. Phys. Chem. Lett.*, 2015, **6**, 4297–4302.
75 R. L. Z. Hoye, R. E. Brandt, A. Osherov, V. Stevanović, S. D. Stranks, M. W. B. Wilson, H. Kim, A. J. Akey, J. D. Perkins, R. C. Kurchin, J. R. Poindexter, E. N. Wang, M. G. Bawendi, V. Bulović and T. Buonassisi, *Chem. – Eur. J.*, 2016, **22**, 2605–2610.
76 R. E. Brandt, V. Stevanović, D. S. Ginley and T. Buonassisi, *MRS Commun.*, 2015, **5**, 265–275.
77 J. Burschka, N. Pellet, S. J. Moon, R. Humphry-Baker, P. Gao, M. K. Nazeeruddin and M. Gratzel, *Nature*, 2013, **499**, 316–319.
78 Q. Chen, H. Zhou, Z. Hong, S. Luo, H.-S. Duan, H.-H. Wang, Y. Liu, G. Li and Y. Yang, *J. Am. Chem. Soc.*, 2014, **136**, 622–625.
79 J. S. Manser, M. I. Saidaminov, J. A. Christians, O. M. Bakr and P. V. Kamat, *Acc. Chem. Res.*, 2016, **49**, 330–338.
80 B. Philippe, B. W. Park, R. Lindblad, J. Oscarsson, S. Ahmadi, E. M. J. Johansson and H. Rensmo, *Chem. Mater.*, 2015, **27**, 1720–1731.
81 Y. Zhao and K. Zhu, *J. Phys. Chem. Lett.*, 2014, **5**, 4175–4186.
82 N. J. Jeon, J. H. Noh, Y. C. Kim, W. S. Yang, S. Ryu and S. Il Seol, *Nat. Mater.*, 2014, **13**, 897–903.
83 M. D. Xiao, F. Z. Huang, W. C. Huang, Y. Dkhissi, Y. Zhu, J. Etheridge, A. Gray-Weale, U. Bach, Y. B. Cheng and L. Spiccia, *Angew. Chem., Int. Ed.*, 2014, **53**, 9898–9903.
84 X. Li, D. Q. Bi, C. Y. Yi, J. D. Decoppet, J. S. Luo, S. M. Zakeeruddin, A. Hagfeldt and M. Gratzel, *Science*, 2016, **353**, 58–62.
85 W. D. Zhu, T. Yu, F. M. Li, C. X. Bao, H. Gao, Y. Yi, J. Yang, G. Fu, X. X. Zhou and Z. G. Zou, *Nanoscale*, 2015, **7**, 5427–5434.
86 Z. G. Xiao, Q. F. Dong, C. Bi, Y. C. Shao, Y. B. Yuan and J. S. Huang, *Adv. Mater.*, 2014, **26**, 6503–6509.
87 S. Yang, Y. C. Zheng, Y. Hou, X. Chen, Y. Chen, Y. Wang, H. J. Zhao and H. G. Yang, *Chem. Mater.*, 2014, **26**, 6705–6710.
88 W. Z. Li, J. D. Fan, J. W. Li, Y. H. Mai and L. D. Wang, *J. Am. Chem. Soc.*, 2015, **137**, 10399–10405.
89 H. Miyamae, Y. Numahata and M. Nagata, *Chem. Lett.*, 1980, 663–664.
90 Y. L. Guo, K. Shoyama, W. Sato, Y. Matsuo, K. Inoue, K. Harano, C. Liu, H. Tanaka and E. Nakamura, *J. Am. Chem. Soc.*, 2015, **137**, 15907–15914.
91 N. Ahn, D. Y. Son, I. H. Jang, S. M. Kang, M. Choi and N. G. Park, *J. Am. Chem. Soc.*, 2015, **137**, 8696–8699.
92 J. W. Lee, H. S. Kim and N. G. Park, *Acc. Chem. Res.*, 2016, **49**, 311–319.
93 Y. G. Rong, S. Venkatesan, R. Guo, Y. N. Wang, J. M. Bao, W. Z. Li, Z. Y. Fan and Y. Yao, *Nanoscale*, 2016, **8**, 12892–12899.
94 Y. C. Kim, N. J. Jeon, J. H. Noh, W. S. Yang, J. Seo, J. S. Yun, A. Ho-Baillie, S. Huang, M. A. Green, J. Seidel, T. K. Ahn and S. Il Seok, *Adv. Energy Mater.*, 2016, **6**, 1502104.
95 Q. Chen, H. Zhou, T.-B. Song, S. Luo, Z. Hong, H.-S. Duan, L. Dou, Y. Liu and Y. Yang, *Nano Lett.*, 2014, **14**, 4158–4163.
96 S. Wang, W. Dong, X. Fang, Q. Zhang, S. Zhou, Z. Deng, R. Tao, J. Shao, R. Xia, C. Song, L. Hu and J. Zhu, *Nanoscale*, 2016, **8**, 6600–6608.
97 T. J. Jacobsson, J.-P. Correa-Baena, E. Halvani Anaraki, B. Philippe, S. D. Stranks, M. E. F. Bouduban, W. Tress, K. Schenk, J. Teuscher, J.-E. Moser, H. Rensmo and A. Hagfeldt, *J. Am. Chem. Soc.*, 2016, **138**, 10331–10343.
98 D.-Y. Son, J.-W. Lee, Y. J. Choi, I.-H. Jang, S. Lee, P. J. Yoo, H. Shin, N. Ahn, M. Choi, D. Kim and N.-G. Park, *Nat. Energy*, 2016, **1**, 16081.

99 O. Malinkiewicz, A. Yella, Y. H. Lee, G. M. Espallargas, M. Graetzel, M. K. Nazeeruddin and H. J. Bolink, *Nat. Photonics*, 2014, **8**, 128–132.
100 J.-Y. Jeng, Y.-F. Chiang, M.-H. Lee, S.-R. Peng, T.-F. Guo, P. Chen and T.-C. Wen, *Adv. Mater.*, 2013, **25**, 3727–3732.
101 S. Sun, T. Salim, N. Mathews, M. Duchamp, C. Boothroyd, G. Xing, T. C. Sum and Y. M. Lam, *Energy Environ. Sci.*, 2014, **7**, 399–407.
102 W. Nie, H. Tsai, R. Asadpour, J.-C. Blancon, A. J. Neukirch, G. Gupta, J. J. Crochet, M. Chhowalla, S. Tretiak, M. A. Alam, H.-L. Wang and A. D. Mohite, *Science*, 2015, **347**, 522–525.
103 W. Chen, Y. Wu, Y. Yue, J. Liu, W. Zhang, X. Yang, H. Chen, E. Bi, I. Ashraful, M. Grätzel and L. Han, *Science*, 2015, **350**, 944–948.
104 Z. Zhu, Y. Bai, X. Liu, C.-C. Chueh, S. Yang and A. K. Y. Jen, *Adv. Mater.*, 2016, **28**, 6478–6484.
105 W. Yan, S. Ye, Y. Li, W. Sun, H. Rao, Z. Liu, Z. Bian and C. Huang, *Adv. Energy Mater.*, 2016, **6**, 1600474.
106 K. Domanski, J.-P. Correa-Baena, N. Mine, M. K. Nazeeruddin, A. Abate, M. Saliba, W. Tress, A. Hagfeldt and M. Grätzel, *ACS Nano*, 2016, **10**, 6306–6314.
107 J.-H. Im, C.-R. Lee, J.-W. Lee, S.-W. Park and N.-G. Park, *Nanoscale*, 2011, **3**, 4088–4093.
108 M. M. Lee, J. Teuscher, T. Miyasaka, T. N. Murakami and H. J. Snaith, *Science*, 2012, **338**, 643–647.
109 J. Burschka, N. Pellet, S.-J. Moon, R. Humphry-Baker, P. Gao, M. K. Nazeeruddin and M. Grätzel, *Nature*, 2013, **499**, 316–319.
110 N. J. Jeon, J. H. Noh, Y. C. Kim, W. S. Yang, S. Ryu and S. I. Seok, *Nat. Mater.*, 2014, **13**, 897–903.
111 W. S. Yang, J. H. Noh, N. J. Jeon, Y. C. Kim, S. Ryu, J. Seo and S. I. Seok, *Science*, 2015, **348**, 1234–1237.
112 M. Liu, M. B. Johnston and H. J. Snaith, *Nature*, 2013, **501**, 395–398.
113 H. Zhou, Q. Chen, G. Li, S. Luo, T.-b. Song, H.-S. Duan, Z. Hong, J. You, Y. Liu and Y. Yang, *Science*, 2014, **345**, 542–546.
114 N. N. C. F. P. H. Page, http://www.nrel.gov/ncpv, (accessed July 30, 2016).
115 H.-S. Kim, C.-R. Lee, J.-H. Im, K.-B. Lee, T. Moehl, A. Marchioro, S.-J. Moon, R. Humphry-Baker, J.-H. Yum, J. E. Moser, M. Grätzel and N.-G. Park, *Sci. Rep.*, 2012, **2**, 591.
116 D. Bi, C. Yi, J. Luo, J.-D. Décoppet, F. Zhang, S. M. Zakeeruddin, X. Li, A. Hagfeldt and M. Grätzel, *Nat. Energy*, 2016, **1**, 16142.
117 M. Saliba, S. Orlandi, T. Matsui, S. Aghazada, M. Cavazzini, J.-P. Correa-Baena, P. Gao, R. Scopelliti, E. Mosconi, K.-H. Dahmen, F. De Angelis, A. Abate, A. Hagfeldt, G. Pozzi, M. Graetzel and M. K. Nazeeruddin, *Nat. Energy*, 2016, **1**, 15017.
118 J.-P. Correa-Baena, M. Anaya, G. Lozano, W. Tress, K. Domanski, M. Saliba, T. Matsui, T. J. Jacobsson, M. E. Calvo, A. Abate, M. Grätzel, H. Míguez and A. Hagfeldt, *Adv. Mater.*, 2016, **28**, 5031–5037.
119 J.-Y. Seo, T. Matsui, J. Luo, J.-P. Correa-Baena, F. Giordano, M. Saliba, K. Schenk, A. Ummadisingu, K. Domanski, M. Hadadian, A. Hagfeldt, S. M. Zakeeruddin, U. Steiner, M. Grätzel and A. Abate, *Adv. Energy Mater.*, 2016, **6**, 1600767.
120 D. Yang, X. Zhou, R. Yang, Z. Yang, W. Yu, X. Wang, C. Li, S. Liu and R. P. H. Chang, *Energy Environ. Sci.*, 2016, **9**, 3071–3078.
121 S. Ameen, M. A. Rub, S. A. Kosa, K. A. Alamry, M. S. Akhtar, H.-S. Shin, H.-K. Seo, A. M. Asiri and M. K. Nazeeruddin, *ChemSusChem*, 2016, **9**, 10–27.
122 P. Dhingra, P. Singh, P. J. S. Rana, A. Garg and P. Kar, *Energy Technol.*, 2016, **4**, 891–938.
123 T. Swetha and S. P. Singh, *J. Mater. Chem. A*, 2015, **3**, 18329–18344.
124 C. H. Teh, R. Daik, E. L. Lim, C. C. Yap, M. A. Ibrahim, N. A. Ludin, K. Sopian and M. A. Mat Teridi, *J. Mater. Chem. A*, 2016, **4**, 15788–15822.
125 Z. Yu and L. Sun, *Adv. Energy Mater.*, 2015, **5**, 1500213.
126 N. J. Jeon, H. G. Lee, Y. C. Kim, J. Seo, J. H. Noh, J. Lee and S. I. Seok, *J. Am. Chem. Soc.*, 2014, **136**, 7837–7840.
127 T. Malinauskas, D. Tomkute-Luksiene, R. Sens, M. Daskeviciene, R. Send, H. Wonneberger, V. Jankauskas, I. Bruder and V. Getautis, *ACS Appl. Mater. Interfaces*, 2015, **7**, 11107–11116.
128 A. Abate, T. Leijtens, S. Pathak, J. Teuscher, R. Avolio, M. E. Errico, J. Kirkpatrik, J. M. Ball, P. Docampo, I. McPherson and H. J. Snaith, *Phys. Chem. Chem. Phys.*, 2013, **15**, 2572–2579.
129 A. Abate, D. R. Staff, D. J. Hollman, H. J. Snaith and A. B. Walker, *Phys. Chem. Chem. Phys.*, 2014, **16**, 1132–1138.
130 S. Park, J. H. Heo, J. H. Yun, T. S. Jung, K. Kwak, M. J. Ko, C. H. Cheon, J. Y. Kim, S. H. Im and H. J. Son, *Chem. Sci.*, 2016, **7**, 5517–5522.
131 A. Mei, X. Li, L. Liu, Z. Ku, T. Liu, Y. Rong, M. Xu, M. Hu, J. Chen, Y. Yang, M. Grätzel and H. Han, *Science*, 2014, **345**, 295–298.
132 X. Li, M. Tschumi, H. Han, S. S. Babkair, R. A. Alzubaydi, A. A. Ansari, S. S. Habib, M. K. Nazeeruddin, S. M. Zakeeruddin and M. Grätzel, *Energy Technol.*, 2015, **3**, 551–555.
133 S. Gholipour, J.-P. Correa-Baena, K. Domanski, T. Matsui, L. Steier, F. Giordano, F. Tajabadi, W. Tress, M. Saliba, A. Abate, A. Morteza Ali, N. Taghavinia, M. Grätzel and A. Hagfeldt, *Adv. Energy Mater.*, 2016, **6**, 1601116.
134 C.-Y. Chan, Y. Wang, G.-W. Wu and E. Wei-Guang Diau, *J. Mater. Chem. A*, 2016, **4**, 3872–3878.
135 S. N. Habisreutinger, T. Leijtens, G. E. Eperon, S. D. Stranks, R. J. Nicholas and H. J. Snaith, *Nano Lett.*, 2014, **14**, 5561–5568.
136 K. Aitola, K. Sveinbjornsson, J.-P. Correa-Baena, A. Kaskela, A. Abate, Y. Tian, E. M. J. Johansson, M. Gratzel, E. I. Kauppinen, A. Hagfeldt and G. Boschloo, *Energy Environ. Sci.*, 2016, **9**, 461–466.
137 P. Qin, S. Tanaka, S. Ito, N. Tetreault, K. Manabe, H. Nishino, M. K. Nazeeruddin and M. Grätzel, *Nat. Commun.*, 2014, **5**, 3834.
138 J. M. Ball, S. D. Stranks, M. T. Horantner, S. Huttner, W. Zhang, E. J. W. Crossland, I. Ramirez, M. Riede, M. B. Johnston, R. H. Friend and H. J. Snaith, *Energy Environ. Sci.*, 2015, **8**, 602–609.

139 S. De Wolf, J. Holovsky, S.-J. Moon, P. Löper, B. Niesen, M. Ledinsky, F.-J. Haug, J.-H. Yum and C. Ballif, *J. Phys. Chem. Lett.*, 2014, **5**, 1035–1039.
140 A. Dualeh, T. Moehl, N. Tétreault, J. Teuscher, P. Gao, M. K. Nazeeruddin and M. Grätzel, *ACS Nano*, 2014, **8**, 362–373.
141 H.-S. Kim and N.-G. Park, *J. Phys. Chem. Lett.*, 2014, **5**, 2927–2934.
142 Y. Shao, Z. Xiao, C. Bi, Y. Yuan and J. Huang, *Nat. Commun.*, 2014, **5**, 5784.
143 C. Eames, J. M. Frost, P. R. F. Barnes, B. C. O'Regan, A. Walsh and M. S. Islam, *Nat. Commun.*, 2015, **6**, 7497.
144 S. Meloni, T. Moehl, W. Tress, M. Franckevicius, M. Saliba, Y. H. Lee, P. Gao, M. K. Nazeeruddin, S. M. Zakeeruddin, U. Rothlisberger and M. Graetzel, *Nat. Commun.*, 2016, **7**, 10334.
145 C. Li, S. Tscheuschner, F. Paulus, P. E. Hopkinson, J. Kiessling, A. Kohler, Y. Vaynzof and S. Huettner, *Adv. Mater.*, 2016, **28**, 2446–2454.
146 T.-Y. Yang, G. Gregori, N. Pellet, M. Grätzel and J. Maier, *Angew. Chem., Int. Ed.*, 2015, **54**, 7905–7910.
147 L. Etgar, P. Gao, Z. Xue, Q. Peng, A. K. Chandiran, B. Liu, M. K. Nazeeruddin and M. Grätzel, *J. Am. Chem. Soc.*, 2012, **134**, 17396–17399.
148 K. Tvingstedt, O. Malinkiewicz, A. Baumann, C. Deibel, H. J. Snaith, V. Dyakonov and H. J. Bolink, *Sci. Rep.*, 2014, **4**, 6071.
149 W. Tress, N. Marinova, O. Inganäs, M. K. Nazeeruddin, S. M. Zakeeruddin and M. Graetzel, *Adv. Energy Mater.*, 2015, **5**, 1400812.
150 D. Liu, J. Yang and T. L. Kelly, *J. Am. Chem. Soc.*, 2014, **136**, 17116–17122.
151 N. Marinova, W. Tress, R. Humphry-Baker, M. I. Dar, V. Bojinov, S. M. Zakeeruddin, M. K. Nazeeruddin and M. Grätzel, *ACS Nano*, 2015, **9**, 4200–4209.
152 M. B. Johnston and L. M. Herz, *Acc. Chem. Res.*, 2016, **49**, 146–154.
153 T. Ishihara, *J. Lumin.*, 1994, **60**, 269–274.
154 T. Umebayashi, K. Asai, T. Kondo and A. Nakao, *Phys. Rev. B: Condens. Matter Mater. Phys.*, 2003, **67**, 155405.
155 W.-J. Yin, T. Shi and Y. Yan, *Appl. Phys. Lett.*, 2014, **104**, 063903.
156 D. Pérez-del-Rey, D. Forgács, E. M. Hutter, T. J. Savenije, D. Nordlund, P. Schulz, J. J. Berry, M. Sessolo and H. J. Bolink, *Adv. Mater.*, 2016, **28**, 1521–4095.
157 J. Emara, T. Schnier, N. Pourdavoud, T. Riedl, K. Meerholz and S. Olthof, *Adv. Mater.*, 2015, **28**, 1521–4095.
158 C. Wehrenfennig, G. E. Eperon, M. B. Johnston, H. J. Snaith and L. M. Herz, *Adv. Mater.*, 2014, **26**, 1584–1589.
159 G. Xing, N. Mathews, S. Sun, S. S. Lim, Y. M. Lam, M. Grätzel, S. Mhaisalkar and T. C. Sum, *Science*, 2013, **342**, 344–347.
160 S. D. Stranks, G. E. Eperon, G. Grancini, C. Menelaou, M. J. Alcocer, T. Leijtens, L. M. Herz, A. Petrozza and H. J. Snaith, *Science*, 2013, **342**, 341–344.
161 C.-G. Wu, C.-H. Chiang, Z.-L. Tseng, M. K. Nazeeruddin, A. Hagfeldt and M. Gratzel, *Energy Environ. Sci.*, 2015, **8**, 2725–2733.
162 P. Schulz, E. Edri, S. Kirmayer, G. Hodes, D. Cahen and A. Kahn, *Energy Environ. Sci.*, 2014, **7**, 1377–1381.
163 A. Guerrero, E. J. Juarez-Perez, J. Bisquert, I. Mora-Sero and G. Garcia-Belmonte, *Appl. Phys. Lett.*, 2014, **105**, 133902.
164 J. M. Azpiroz, E. Mosconi, J. Bisquert and F. De Angelis, *Energy Environ. Sci.*, 2015, **8**, 2118–2127.
165 E. M. Miller, Y. Zhao, C. C. Mercado, S. K. Saha, J. M. Luther, K. Zhu, V. Stevanovic, C. L. Perkins and J. van de Lagemaat, *Phys. Chem. Chem. Phys.*, 2014, **16**, 22122–22130.
166 L. E. Polander, P. Pahner, M. Schwarze, M. Saalfrank, C. Koerner and K. Leo, *APL Mater.*, 2014, **2**, 081503.
167 R. A. Belisle, P. Jain, R. Prasanna, T. Leijtens and M. D. McGehee, *ACS Energy Lett.*, 2016, **1**, 556–560.
168 S. Carli, J. P. C. Baena, G. Marianetti, N. Marchetti, M. Lessi, A. Abate, S. Caramori, M. Grätzel, F. Bellina, C. A. Bignozzi and A. Hagfeldt, *ChemSusChem*, 2016, **9**, 657–661.
169 Z. Song, A. Abate, S. C. Watthage, G. K. Liyanage, A. B. Phillips, U. Steiner, M. Graetzel and M. J. Heben, *Adv. Energy Mater.*, 2016, **6**, 1600846.
170 F. Bella, G. Griffini, J.-P. Correa-Baena, G. Saracco, M. Grätzel, A. Hagfeldt, S. Turri and C. Gerbaldi, *Science*, 2016, **354**, 203–206.
171 A. Abate, S. Paek, F. Giordano, J.-P. Correa-Baena, M. Saliba, P. Gao, T. Matsui, J. Ko, S. M. Zakeeruddin, K. H. Dahmen, A. Hagfeldt, M. Gratzel and M. K. Nazeeruddin, *Energy Environ. Sci.*, 2015, **8**, 2946–2953.
172 M. Kaltenbrunner, G. Adam, E. D. Glowacki, M. Drack, R. Schwodiauer, L. Leonat, D. H. Apaydin, H. Groiss, M. C. Scharber, M. S. White, N. S. Sariciftci and S. Bauer, *Nat. Mater.*, 2015, **14**, 1032–1039.
173 S. Guarnera, A. Abate, W. Zhang, J. M. Foster, G. Richardson, A. Petrozza and H. J. Snaith, *J. Phys. Chem. Lett.*, 2015, **6**, 432–437.
174 T. Matsui, I. Petrikyte, T. Malinauskas, K. Domanski, M. Daskeviciene, M. Steponaitis, P. Gratia, W. Tress, J.-P. Correa-Baena, A. Abate, A. Hagfeldt, M. Grätzel, M. K. Nazeeruddin, V. Getautis and M. Saliba, *ChemSusChem*, 2016, **9**, 2567–2571.
175 B. Roose, J.-P. C. Baena, K. C. Gödel, M. Graetzel, A. Hagfeldt, U. Steiner and A. Abate, *Nano Energy*, 2016, **30**, 517–522.
176 B. Roose, K. C. Gödel, S. Pathak, A. Sadhanala, J. P. C. Baena, B. D. Wilts, H. J. Snaith, U. Wiesner, M. Grätzel, U. Steiner and A. Abate, *Adv. Energy Mater.*, 2016, **6**, 1501868.
177 Z. Xiao, Y. Yuan, Y. Shao, Q. Wang, Q. Dong, C. Bi, P. Sharma, A. Gruverman and J. Huang, *Nat. Mater.*, 2015, **14**, 193–198.
178 M. Hadadian, J.-P. Correa-Baena, E. K. Goharshadi, M. Saliba, A. Ummadisingu, J.-Y. Seo, J. Luo, S. Gholipour, S. M. Zakeeruddin, M. Graetzel, A. Abate and A. Hagfeldt, *Adv. Mater.*, 2016, **28**, 8681–8686.
179 X. Li, M. Ibrahim Dar, C. Yi, J. Luo, M. Tschumi, S. M. Zakeeruddin, M. K. Nazeeruddin, H. Han and M. Grätzel, *Nat. Chem.*, 2015, **7**, 703–711.
180 L. M. Pazos-Outón, M. Szumilo, R. Lamboll, J. M. Richter, M. Crespo-Quesada, M. Abdi-Jalebi, H. J. Beeson, M. Vrućinić, M. Alsari, H. J. Snaith, B. Ehrler, R. H. Friend and F. Deschler, *Science*, 2016, **351**, 1430–1433.
181 M. A. Green, *Prog. Photovoltaics*, 2012, **20**, 472–476.